Acta Geochim (2022) 41(1):100–120
https://doi.org/10.1007/s11631-021-00497-9

ORIGINAL ARTICLE

Geochemical characteristics of Neogene sandstones of the East and West Siang Districts of Arunachal Pradesh, NE India: implications for source-area weathering, provenance, and tectonic setting

Roshmi Boruah[1] · **Jayanta Jivan Laskar**[1]

Received: 30 March 2021 / Revised: 26 August 2021 / Accepted: 29 August 2021 / Published online: 5 October 2021

Abstract Sandstones from the Neogene Siwalik successions of the East and West Siang Districts of Arunachal Pradesh were analyzed to evaluate source-area weathering, provenance, and tectonic setting by using major, trace, and rare earth elements (REEs) as proxies. The sandstones are classified as lithic arenite and wacke arenite based on their mineralogical compositions. The values of different weathering indices such as Chemical Index of Alteration (CIA; 60.93–89.86) and Chemical Index of Weathering (CIW; 40–96.8) suggest moderate to intense weathering in the source area. The plot of Th/Sc versus Zr/Sc indicates enrichment of zircon by sediment sorting and/or recycling from a weathered source. The high positive correlation between Al_2O_3 and K_2O points towards a strong influence of the constituent clay minerals on the major oxide composition of the sandstones. Petrographic analysis together with enriched LREE, flat HREE, negative Eu anomalies (Eu/Eu* = 0.47 to 0.90) in the chondrite-normalized diagrams, and the ratios of La/Sc, La/Co, Th/Sc, Th/Co, Cr/Th collectively suggests that the Neogene sediments were derived from felsic igneous and/or reworked sedimentary/metasedimentary sources in an upper continental crustal setting. The geochemical characteristics of the studied Neogene Siwalik sandstones indicate that the sediments were sourced from pre-Himalayan gneisses and granitoids together with metabasic rocks, which had formed in a passive margin tectonic setup.

✉ Roshmi Boruah
rashmiboruah2011@gmail.com

[1] Department of Geological Sciences, Gauhati University, Guwahati, Assam 781014, India

Keywords Geochemistry · Neogene sandstones · Arunachal Pradesh · Paleo-weathering · Provenance · Tectonic setting

1 Introduction

Geochemical compositions of clastic sediments have been widely used to infer the provenance (Madhavaraju 2015; Odoma et al. 2015; Zaid 2015a, b), paleo-weathering (Rahman et al. 2014; Zaid 2015a, b), and tectonic setting (Armstrong-Altrin et al. 2015; Etemad-Saeed et al. 2015) of their source area. The geochemical characteristics of the sediments are greatly dependent on their grain size, nature of sorting, transport, the intensity of weathering, and the nature of the source rocks (McLennan et al. 1993). Studies on sediment provenance have also revealed that REE and trace elements (Y, Th, Zr, Hf, Nb, Sc, Co, and Cr) remain immobile and do not undergo diagenesis and metamorphism due to their short residence time in seawater and are thus useful in provenance discrimination (Cullers 1994).

Himalayan Neogene sediments in north-east India occur along a thin linear belt in Arunachal Pradesh and are confined between the Main Boundary Thrust (MBT) on the north and the Foot Hill Fault (FHF) on the southern margin (Wadia 1953; Gansser 1964; Mathur and Evans 1964; Karunakaran and Ranga Rao 1976; Tripathi et al. 1988; Geological Survey of India 1989; Kumar 1997; Ramakrishnan and Vaidyanandhan 2008; Kesari 2010; Valdiya 2010). They represent sedimentation in a part of the Himalayan Foreland Basin, which had formed as a result of tectonic loading and crustal sagging in the immediate south of the MBT (Valdiya 2010). The clastic sediment infill was derived from the rapid erosion of the nascent Himalayan Mountains located towards the north of the Himalayan

Foreland Basin (HFB). The fluvial nature of these clastic sediments is reflected in their inherent channel facies (sandstones) and interbedded floodplain facies (mudstone/shale/siltstone) architecture (Sinha et al. 2007). The Neogene sedimentary sequences from different geological sectors of HFB have been studied by different workers (Sinha et al. 2007, 2008; Kundu et al. 2016) and they suggested the Lesser and Higher Himalayan rocks as sources of these sediments. Although much sedimentological and other associated geological study have been undertaken in this portion of the Himalayas, a comprehensive geochemical investigation of the Neogene sandstones in the light of source-rock weathering, provenance, and the tectonic setting is still very much awaited. The present paper discusses various aspects of major and trace element composition of the sandstones belonging to the Dafla and Subansiri Formations of the Neogene Siwalik Group, occurring in the East and West-Siang Districts of Arunachal Pradesh. Sandstone geochemistry has been used to shed light on their provenance, associated paleoweathering, and tectonic setup during sedimentation in the Himalayan Foreland Basin (HFB).

2 Location and geology of the study area

The four established lithotectonic provinces of the Himalayan orogeny are the Tethys Himalaya, Greater Himalaya, Lesser Himalaya, and Sub-Himalaya (more commonly known as 'the Siwaliks'), which occur sequentially from north to south along with thrusts that are named as South Tibetan Detachment (STD), Main Central Thrust (MCT), Main Boundary Thrust (MBT) and Himalayan Frontal Thrust (HFT) respectively (Valdiya 1980; Yin et al. 2006). The Sub-Himalaya is thrust southward over the Brahmaputra alluvium along Himalayan Frontal Thrust (HFT) in this part of the Himalaya (Karunakaran and Ranga Rao 1976). In the north, the Lesser Himalaya is thrust over the Sub-Himalaya along with the MBT and this rock succession comprises Precambrian to Cambrian low to medium grade metasedimentary rocks such as granites and granitic gneisses. Further North, the MCT places the Greater Himalaya over the Lesser Himalaya and comprises of high-grade metamorphic rocks intruded pervasively by Early Miocene granites. The Tethys Himalaya lies in between the STD in the south and the Indus-Tsangpo suture zone in the north and comprises of Late Proterozoic-Eocene low grade metamorphic and sedimentary rock succession (Auden 1934; Gansser 1964).

The Neogene Siwalik Group of rocks of East and West Siang Districts, Arunachal Pradesh comprises the southernmost litho-tectonic belt and is delimited by the Brahmaputra alluvium and Quaternary deposits in the south and by Gondwana rocks in the North. The latter is thrust against the Siwalik belt along the Main Boundary Thrust (MBT). This linear belt of Neogene sediments extends from Bhutan in the West to just east of Pasighat along the foothills where it is overlapped by alluvium and is exposed along the ENE–WSW to NE–SW trending sub-Himalayan belt. In the Arunachal foothills, this Neogene (Siwalik) sequence is classified into Dafla Formation (DF), Subansiri Formation (SF), and the Kimin Formation (KF), which are further correlated with the Lower, Middle and Upper sub-divisions of the Siwalik Group of the northwestern Himalaya (Karunakaran and Ranga Rao 1976). The stratigraphic succession of the Neogene sediments of the study area is described in Table 1 and the location map of the study area is shown in Fig. 1. Sekhose et al. (2016) also correlated the Siwalik sequence with the Tertiary sequence of Naga-Patkai belt; wherein the Kimin is correlated with Dihing, Subansiri with Tipam, and Dafla with Bokabil Formations of Assam, Manipur, Mizoram, and Nagaland. It is also sometimes considered as the northward extension of the Tertiary sequence of Assam. In the Likabali area, the Neogene sediments attain a maximum thickness greater than 7 km (Mathur and Evans 1964; Karunakaran and Ranga Rao 1976). A significant difference observed in the characteristics of the Neogene sediments of the eastern Himalaya with those occurring in other parts of the Himalayan terrain is the rarity of terrestrial vertebrate fossils, which otherwise are present in most Neogene (Siwalik) sequences of the western Himalaya. For instance, Singh (1977) reported a mammalian vertebrate fossil of Boss sp., in the Arunachal Himalaya. Some representative field photographs showing various lithofacies varieties found in DF and SF are described in Fig. 2. In the field, the sandstones belonging to the DF are observed to be semi-indurated to indurated, fine to medium-grained, brown to pale brown, grey to greenish-grey colored sandstones, with subordinate amounts of carbonaceous shales, mudstones, and alterations of sandstones and shales. There are embedded cobbles and boulders of mudstone, sandstone, and quartzites, together with discontinuous coal streaks and deposits of reddish ferruginous material within the grey-colored sandstones. The SF comprises massive to bedded friable sandstones which exhibit a "salt and pepper" texture. There are embedded pebbles and boulders in the sandstones, some of which are well rounded in shape. The transition from SF to KF is characterized by the reappearance of mudstones and siltstones interlayered with thin sandstones and thicker conglomerate beds (Chirouze et al. 2012; Lang et al. 2016; Taral et al. 2017). Magnetostratigraphy of the Neogene sediments in the Kameng section indicates their time of deposition to be between 13 and 2.5 Ma. The transition from Lower to Middle Neogene sedimentation occurred at

Table 1 Stratigraphic succession of Neogene sediments of Eastern Himalayan belt (after Kesari 2010)

	Age	Group	Formation	Lithology
	Holocene to Recent	Quaternary Sediments	Hapoli Formation (Newer Alluvium)	Sand, Clay and peat
	Middle to Upper Pleistocene		Older Alluvium	Unconsolidated sediments represented by boulders, cobble, pebble, sand and sandy clay beds
	Main Frontal Thrust			
	Mio-Pliocene	Siwalik Group	Kimin Formation (Upper Siwalik)	Boulder conglomerate, pebble sandstone
Study area	**Mio-Pliocene**		**Subansiri Formation (Middle Siwalik)**	**Salt and peppery lithic arenite**
	Miocene		**Dafla Formation (Lower Siwalik)**	**Micaceous sandstone with calcareous concretions.**
	Main Boundary Thrust			

10.5 Ma while the transition from Middle to Upper Neogene sedimentation took place at 2.6 Ma (Chirouze et al. 2012). In the Eastern Arunachal Himalaya, the Higher Himalaya is represented by the Sela Group and comprises mainly of migmatites, garnetiferous gneiss, calc-gneiss/marble, staurolite schist, and quartzites while the Lesser Himalayan sequences are represented by the low to medium grade Dirang/Lumla Formation and Bomdila Gneiss. The Dirang/Lumla Formation comprises low to medium-grade meta-sedimentary rocks such as garnetiferous mica schist, phyllites, quartzites, and marble, while the Bomdila Gneiss consists mainly of porphyritic granitic gneiss (Bhattacharjee and Nandy 2009). Chirouze et al. (2013) also carried out isotopic studies and concluded that the Siwalik sediments were mostly derived from Higher Himalayan sources and Gangdese Batholith and Yarlung suture zone through the Brahmaputra river system.

3 Methodology

Sandstone samples were collected from DF and SF which are exposed along the Garu-Likabali road section and Demow river section of West Siang District and Simen and Rayang river sections of East Siang District of Arunachal Pradesh. A total of twenty-five (25) sandstone samples representing the DF and SF were selected for petrographic and geochemical analysis, by avoiding the weathered and jointed surfaces. The fresh un-weathered samples were crushed in an agate mortar and powdered to 200 ASTM mesh to maintain the uniformity of the samples. The samples were then analyzed for major, trace, and rare earth elements (REE) in the geochemical laboratory at Geochemistry Division, CSIR- National Geophysical Research Institute, Hyderabad. The major oxides were analyzed with X-ray Fluorescence (XRF) spectrometer (Axios model, PAN analytical), using pressed pellet following procedures described in Saini et al. (2000). The trace elements including REE were analyzed with a High Resolution Inductively Coupled Plasma Mass Spectrometer (HR-ICP-MS; ATTOM model, Nu Instruments, UK), using an open acid digestion technique. The methodologies suggested by Krishna et al. (2007) and Satyanarayanan et al. (2014) were followed for XRF and HR-ICP-MS respectively. Geological Standard Reference, GSR—4 was used as an internal standard to monitor the quality of the data. The accuracy and precision of major oxides and trace elements are $< 3\%$ and better than 2% respectively. The details of precision and accuracy protocols for major and trace element analyses were described respectively in Krishna et al. (2007) and Satyanarayanan et al. (2014).

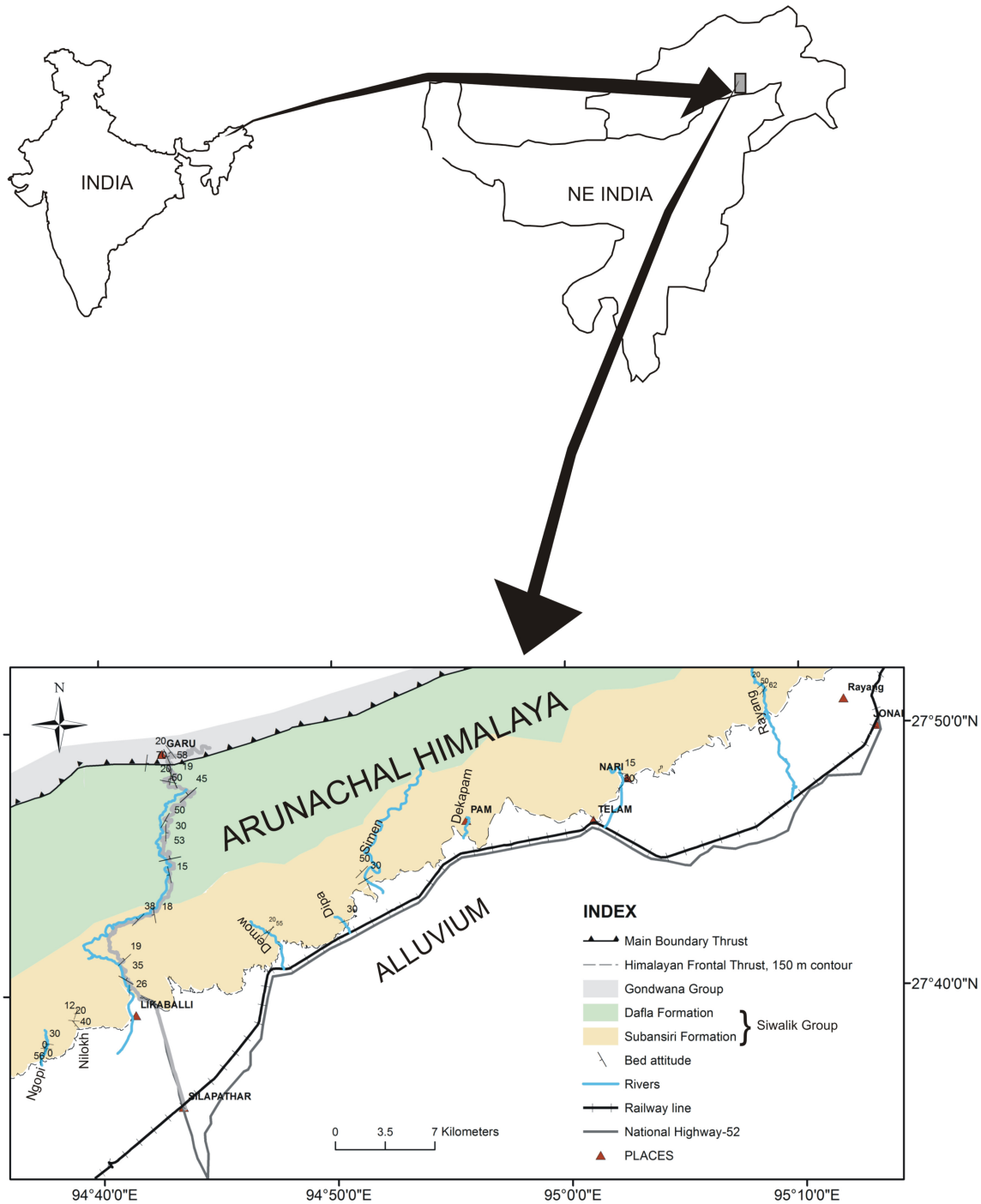

Fig. 1 Location map of the study area

4 Results

4.1 Petrography

Thin section petrography of DF and SF sandstones indicates an interlocking framework of sub-angular and sub-rounded quartz (monocrystalline, Qm and polycrystalline, Qp), K-feldspar, plagioclase, and lithic fragments consisting of both sedimentary and metamorphic rocks. Quartz is more abundant than feldspar and lithic fragments in the sandstones of both DF and SF, and no contrasting change in their mineralogical composition could be identified. The quartz grains are commonly sub-rounded to sub-angular in shape and constitute ~ 50%–60% of the volume of rock. Among quartz grains, Qm (Fig. 3A, E) was dominant over Qp. Qm grains were mostly non-undulatory

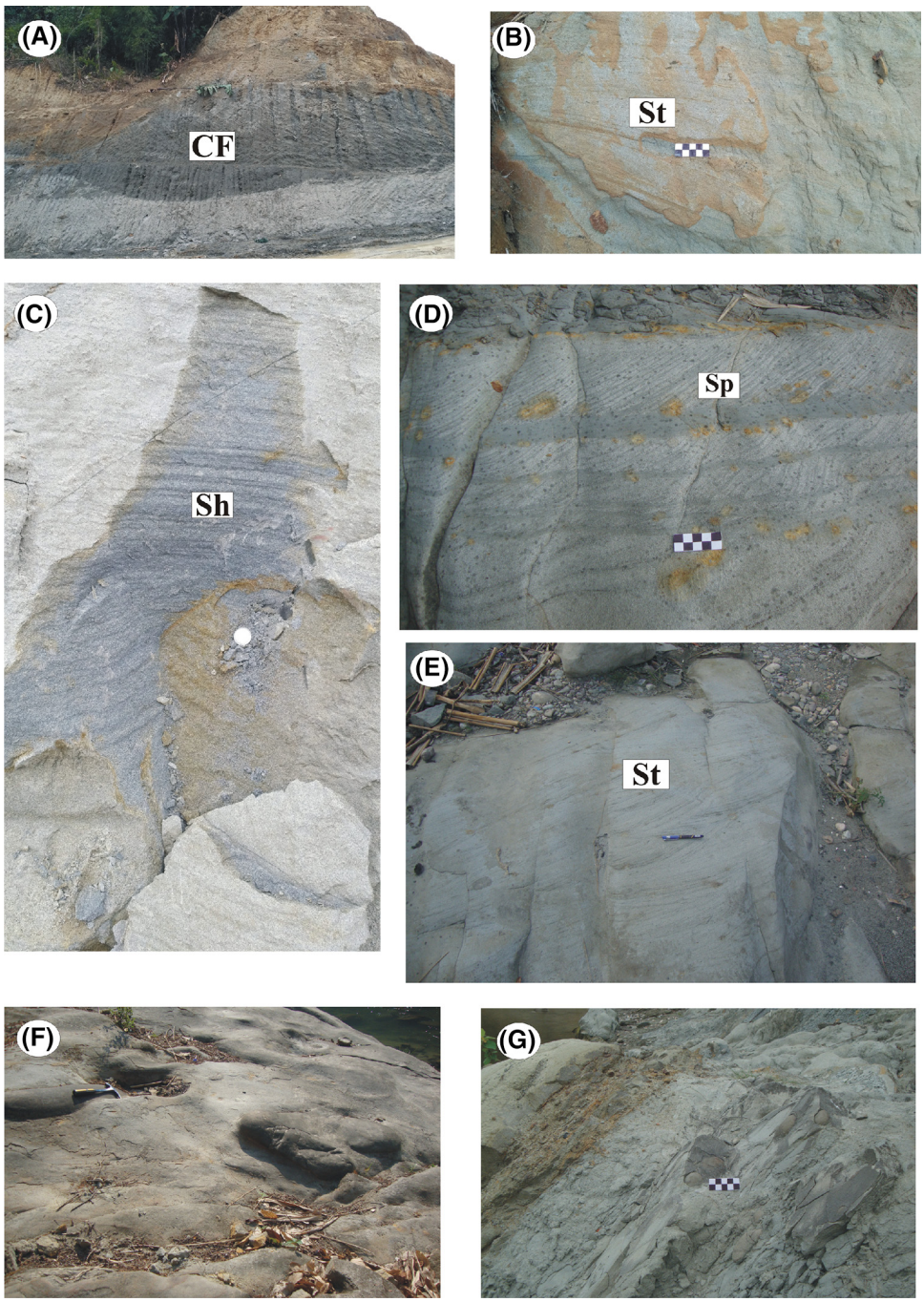

Fig. 2 Field photographs showing some representative lithofacies of DF (**A**—a channel-fill (CF) deposit marked by a thin greenish muddy layer (average thickness—6 cm) with an erosional top surface; **B**—trough cross-bedded (St) grey coloured sandstone; **C**—horizontal stratification (Sh) in grey coloured sandstone) and SF (**D**—planar cross-bedded (Sp) grey coloured sandstone; **E**—trough cross-bedding (St) within the pebbly bedded grey medium grained sandstone. The sandstone contains innumerable red and brownish grey coloured mud and sand clasts with few coal streaks; **F**—Huge embedded clasts of sandstone in massive, jointed grey coloured sandstone. Clasts are of boulder size with their long diameter varying from 82 to 120 cm; **G**—Rounded embedded sandstone clasts in sandstone bed. Longest diameter ranges from 2.5 to 12 cm) in the study area)

while a few were undulose in nature. Quartz grains were observed with point, concavo-convex contact, sutured contact, and straight contact boundary.

Lithic fragments are the second most abundant framework grains which make up ~ 20%–30% of the total framework grain population. They are variable in size, angular to sub-angular, with prominent grain boundaries. They are represented by both metamorphic lithic fragments (Fig. 3B) such as quartzite, mica-schist, gneiss, phyllite, and sedimentary lithic fragments (Fig. 3B) such as siltstone, shale, sandstone, mudstone. Feldspars constitute a meager population of about ~ 5%–7% of the total framework grain and comprise both potash (K) and plagioclase feldspars. Potash feldspars (Fig. 3A) are comparatively more dominant than plagioclase feldspars. Unaltered as well as partially altered feldspars are observed in the thin sections. At places, feldspars are corroded by calcareous cement and often contribute to the formation of matrix. Matrix (Fig. 3B) is observed in all the thin sections. The dissolution of less-resistant grains in some thin

sections probably contributes to the formation of matrix in the mineralogical framework. They comprise an average of 12.2% and 6.03% of the framework composition of the sandstones belonging to the DF and SF respectively. Besides matrix, cement is also present with some being present along with fractures of quartz and feldspar grains. Calcite cement (Fig. 3C, F) mostly sporadic and less commonly micrite, silica (Fig. 3E), and ferruginous cement are also observed. At places, the boundaries of quartz grains are observed to be irregular (i.e. corroded) which might be due to its reaction with the surrounding calcitic cement. This may also indicate the precipitation of calcites in the sandstones after deposition of the sediments.

Apart from the major framework mineral constituents, accessory minerals are present in minor amounts and include biotite, muscovite (Fig. 3B), chlorite (Fig. 3C), andalusite, garnet (Fig. 3C), hornblende (Fig. 3D), sphene (Fig. 3E), tourmaline, zircon (Fig. 3D) and a few opaque grains. Micas are mostly bent as well as kinked and dominate the accessory mineral population.

4.2 Geochemistry

4.2.1 Major elements

The concentrations (in wt%) of the major element oxides of sandstones of DF and SF are given in Tables S1 and S2 (supplementary material), respectively. The tabulated data indicates that SiO_2, Al_2O_3, and Fe_2O_3 form the major bulk of the geochemical composition of the analyzed samples. The proportion of SiO_2 ranges between 60.92% and 71.54% (average 66.77%) in DF, and 51.99%–76.03% (average 64.22%) in SF, suggesting high quartz content. In DF, Al_2O_3 ranges between 11.5% and 16.84% (average 13.97%), while it is between 11.43% and 17.41% (average 14.03%) in SF, which may be due to the presence of clay as well as other micaceous minerals in them. Their K_2O (1.6%–2.2%: DF; 1.09%–2.37%: SF) and Na_2O (0.31%–1.19%: DF; 0.79%–2.92%: SF) content suggests the dominance of orthoclase over plagioclase feldspars which is also supported by their petrographic observations. In DF, Fe_2O_3 contents are between 2.74% and 7.06% (average 4.68%) and it varies between 1.98% and 18.49% (average 6.63%) in SF. CaO also shows significant variation in both DF and SF, with ranges of 0.94%–8.97% (average 2.22%) in DF, and 0.03%–10.07% (average 2.55%) in SF.

In DF, only SiO_2 is enriched and all the remaining major element oxides are depleted in comparison to their concentrations in the Upper Continental Crust (UCC; Rudnick and Gao 2003). In SF, Fe_2O_3, MnO, TiO_2 are enriched and the remaining major element oxides are depleted in comparison to their concentration in the UCC as cited in Rudnick and Gao 2003. The significant variations in CaO content and depletion of Na_2O suggest moderate to intense weathering, recycling in the source area, and their removal/addition during transportation. In DF, correlations between SiO_2 with other major oxides show a negative correlation except for Na_2O (Fig. 4). Similar negative correlations between SiO_2 and other major oxides are also evident in SF except for Na_2O and TiO_2 (Fig. 4). This is indicative of free silica being precipitated in the form of quartz. In DF, a good positive correlation is observed between K_2O and Al_2O_3 ($r = 0.73$), indicating their distributions being dominantly controlled by clay minerals such as illite and/or alkali feldspars, whereas in SF no significant correlation is observed ($r = 0.01$). This further suggests decomposition of k-feldspar and muscovite during moderate to strong weathering under humid conditions, the potash getting ultimately fixed within the clays. There might have been a significant contribution of potash from granite and/or granite gneisses (Sinha et al. 2007). The ratio K_2O/Al_2O_3 in sandstone indicates how much alkali feldspar, plagioclase, and clay minerals are present before final burial (Cox et al. 1995). The ratio K_2O/Al_2O_3 in common minerals is alkali feldspars (0.4–1), illite ($\sim$ 0.3), and clay minerals ($\sim$ 0; Cox et al. 1995). The sandstones of DF and SF have an average ratio of 0.14 and 0.13 respectively, suggesting their clay mineral control. This result is also consistent with the low amount of feldspars in the sandstones. Moreover, the presence of fresh, unaltered feldspars indicates that a major amount of clay minerals are transported rather than in-situ origin, which may suggest their derivation from a clay-rich source such as weathered shale, phyllite, and schist (Sinha et al. 2008). Also, the high content of Fe_2O_3 indicates the close association of phyllosilicates which are derived from a biotite-rich source possibly granite and/or phyllite-schist rich provenance. These results are also evident from the presence of sedimentary and metamorphic lithic fragments in petrographic analysis.

The classification diagram of Pettijohn et al. (1972) (Fig. 5A) indicates that the types of sandstones in DF are to be arkose, greywacke, and litharenite, while sandstones of SF are mostly arkosic and litharenitic. However, the plot (Fig. 5B) based on Herron (1988) classifies the DF sediments as mostly wacke, while it classifies the SF sandstones as wacke, shale, and sandstones. Petrographic observations of the sandstones indicate low amounts of feldspars than lithic fragments to classify them as arkose. Thus, Pettijohn's plot does not clearly distinguish litharenite and arkose as compared to Herron's classification. The low Na_2O/K_2O classifies the sandstones as arkose in Pettijohn's plot thereby indicating their immature nature in some samples.

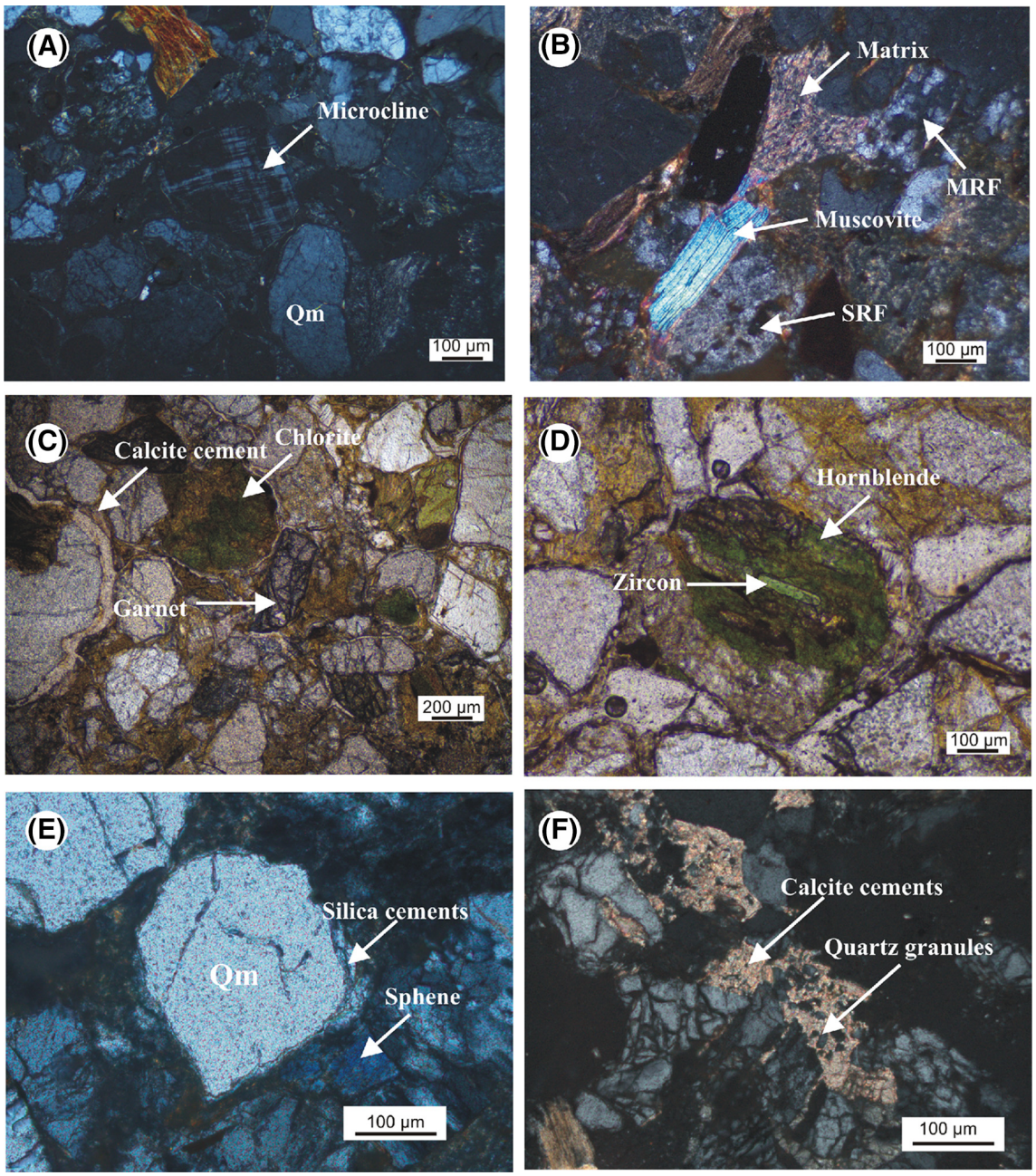

Fig. 3 Photomicrographs of representative sandstone samples of the study area showing framework minerals (quartz, feldspars and rock fragments), matrix, different types of cement (silica and calcite cements), accessory minerals (garnet, zircon, sphene, chlorite, hornblende) and mica minerals (muscovite). Q_m—Monocrystalline quartz, SRF—Sedimentary rock fragment, MRF—Metamorphic rock fragment. The sandstones are dominated by monocrystalline quartz over polycrystalline quartz variety in both the Formations

4.2.2 Trace and rare earth elements

The concentrations of various trace elements present in the Neogene sediments are tabulated in Tables S1 and S2 (supplementary material). The trace element data of the sediments are normalized to UCC cited in Rudnick and Gao (2003) to discuss the possible sources, transportation, and depositional processes of the studied sediments. The multi-element diagrams and REE (Masuda 1962) plot of the Neogene sediments [Fig. 6A–D; Tables S1 and S2 (supplementary material)] reveal that the large ion lithophile elements such as Rb and Cs are enriched in the Neogene DF and SF sediments, while there is depletion in the Sr and Ba contents. This suggests that the sediments have undergone weathering, erosion, and re-depositional cycles which translocated these elements. The High Field Strength Elements (HFSE) such as Th, U, Zr are also enriched but the Transition Trace Elements (TTE) such as

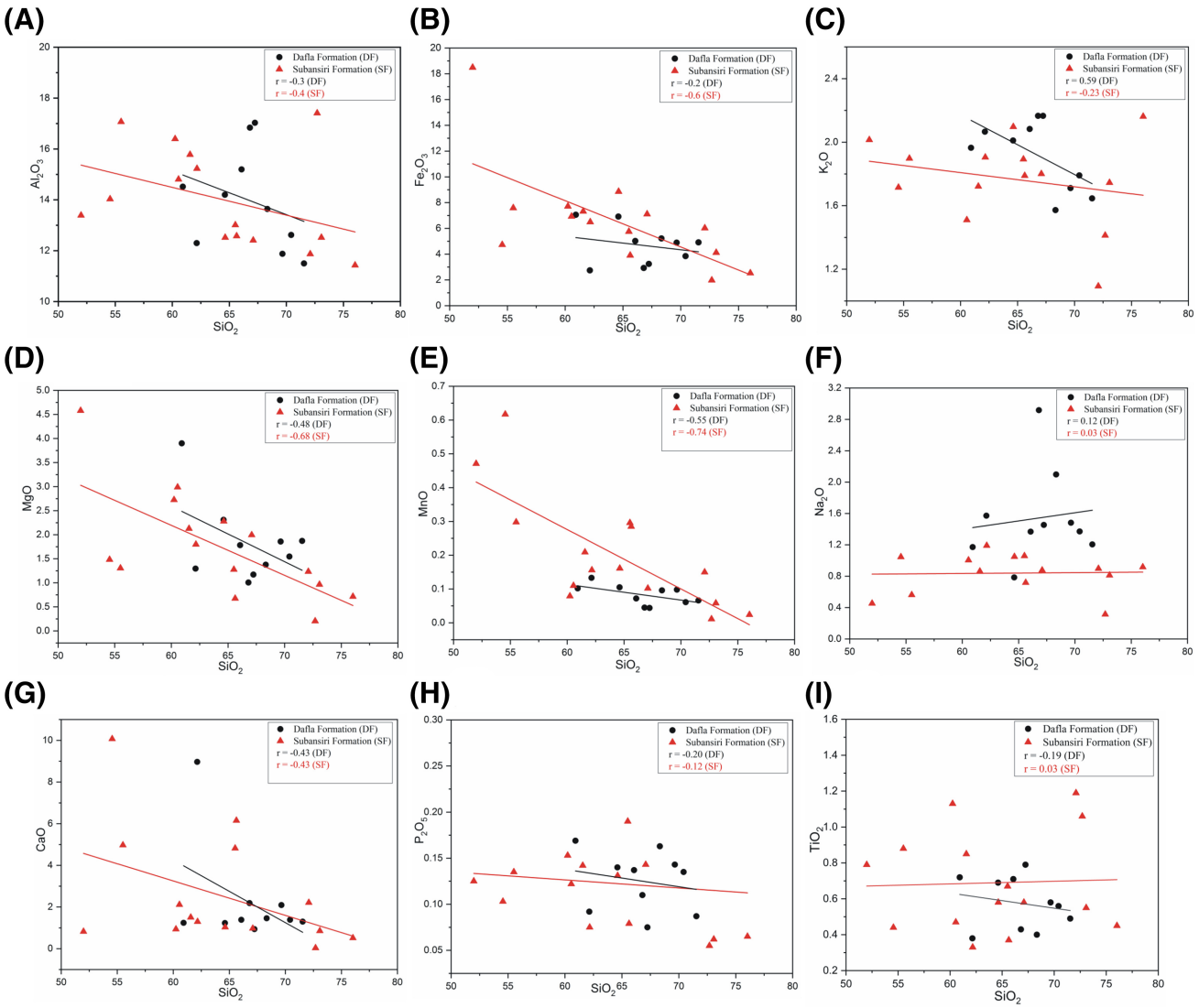

Fig. 4 Harker variation diagrams for major elements in the sandstones of DF and SF in the study area. Note that the datas used in this figures are LOI- free compositions

Cr, V, Co, Ni, and Sc are depleted in comparison to their concentration in the UCC. The total Rare Earth Elements (ΣREE) in DF varies from 133.76 to 225.60 ppm (mean = 180.14 ppm) while in SF it varies from 87.88 ppm to 631.59 ppm (mean = 198.41 ppm). The chondrite normalized plots of REE (Fig. 6C, D) of all the analyzed samples exhibit a uniform trend and are relatively similar to the REE trend of the UCC. They show enrichment in Light Rare Earth Elements (LREE: La-Gd) with a negative Eu anomaly [Eu/Eu* = 0.6–0.7 for DF, and 0.5–0.9 for SF; Tables S1 and S2 (supplementary material)]. The fractionated Heavy Rare Earth Elements (HREE: Tb-Lu) show almost a flat trend. The Eu anomaly was calculated using the formula of McLennan 1989, which states $Eu/Eu^* = Eu/[(Sm)_{CN} \text{ X } (Gd)_{CN}]^{0.5}$, where CN stands for "chondrite normalized".

A correlation analysis amongst various chemical constituents in the sediments was undertaken to identify the existence of significant correlations between various major oxides, trace elements, and REE of the Neogene sediments, with a purpose to understand their mutual influences, and derive inference about associated minerals and rocks. The HFSE such as Rb, Sr, Ba, and Th are positively correlated with Al_2O_3 in the DF (Fig. 7A–D) (Pearson's correlation coefficient, r = 0.90, 0.36, 0.71, 0.62 respectively), indicating that these elements are likely fixed in K-feldspars and clays. On the other hand, the correlation of Al_2O_3 with Rb, Sr, Ba, and Th is very low or insignificant in SF (Fig. 7A–D) (r = 0.37, − 0.01, 0.23, − 0.04 respectively). This suggests that the HFSE is not likely bound in the clay minerals in the SF. Also, a positive correlation is observed between K_2O and Rb, Cs in DF (Fig. 7E, F) (r = 0.89, 0.5

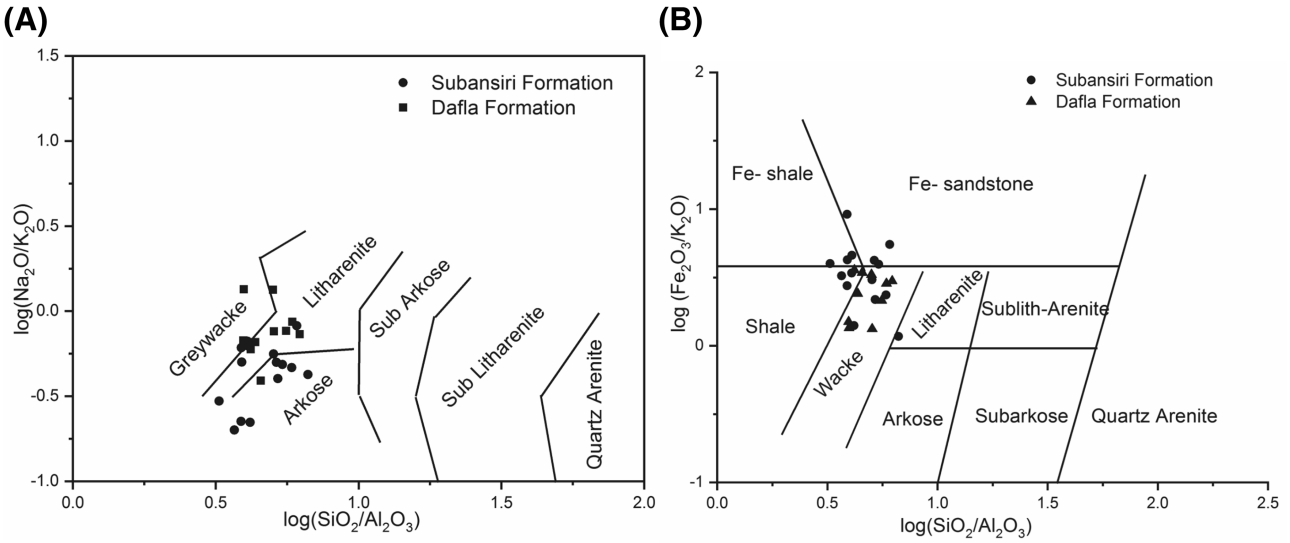

Fig. 5 Geochemical classification diagram (**A**) $log(SiO_2/Al_2O_3)$-$log(Na_2O/K_2O)$ (after Pettijohn et al. 1972) and (**B**) $log(SiO_2/Al_2O_3)$-$log(Fe_2O_3/K_2O)$ (after Herron 1988)

respectively), indicating that clay-bearing minerals (illite) and phyllosilicates (muscovite, biotite) might have controlled the abundance of these trace elements (McLennan et al. 1983; Feng and Kerrich 1990 in Ali et al. 2014). Rb does not show any significant correlation with K_2O in SF (Fig. 7E). The TTE such as Cr, Ni, V does not show a strong correlation with Al_2O_3 in DF (r = 0.21, 0.17, 0.4 respectively), indicating that TTE is not likely fixed in clay minerals. On the other hand in the SF, Cr and V show a positive correlation with Al_2O_3 (r = 0.5, 0.5 respectively), thus indicating that these elements are fixed in clay minerals (Fig. 7G–I). Ni does not show any significant correlation. The sandstones of DF show a positive correlation between K_2O and $\sum$REE (r = 0.53), while it shows a negative correlation in SF (r = − 0.64). This may be suggestive of illite being the host for the REE in DF and negligible influence in SF (Fig. 7J). In addition, $\sum$REE is positively correlated with P_2O_5 in SF (r = 0.79) while the correlation is poor in DF (r = 0.33) (Fig. 7K). This might indicate the influence of phosphate-rich minerals such as apatite in controlling the REE abundance in SF. Also, no significant correlation is observed between Zr and HREE in DF and SF (Fig. 7M) (r = 0.19, 0.13 respectively), suggesting that the concentration of Zr does not influence the HREE content in both the Formations. Both DF and SF show a positive correlation between Zr and TiO_2 (Fig. 7L) (r = 0.74, 0.40 respectively), indicating the presence of certain minerals such as zircon, monazite, ilmenite, and rutile in them.

5 Discussion

5.1 Weathering and Paleoclimatic condition of the source area

To evaluate qualitatively and quantitatively the weathering and paleoclimatic conditions of the source area, Chemical Index of Alteration (CIA; Nesbitt and Young 1982) [$CIA = Al_2O_3/[Al_2O_3 + K_2O + Na_2O + CaO^*) \times 100$], Chemical Index of Weathering (CIW; Harnois 1988) [$CIW = Al_2O_3/[Al_2O_3 + Na_2O + CaO^*) \times 100$], Plagioclase Index of Alteration (PIA; Fedo et al. 1995) [$PIA = [(Al_2O_3 - K_2O)/Al_2O_3 + CaO^* + NaO - K_2O)] \times 100$], etc. have long been used (Armstrong-Altrin et al. 2004; Tang et al. 2012; Ramachandran et al. 2016). The values of major oxides are in molecular proportions and CaO* is the calcium content within the associated silicates. The largest CIA value ($\cong$ 100) is typical of Kaolinite weathering (Nesbitt and Young 1982; Fedo et al. 1995). Values of CIA up to 50 indicate unweathered products, while values ranging between 50 and 70 indicate slight weathering; values between 70 and 80 represent moderate weathering conditions, and values > 80 suggest intense weathering (Nesbitt and Young 1982; Fedo et al. 1995). In the present study, the average CIA values of sandstones belonging to the DF and SF are 67.40 and 75.44 respectively [Tables S1 and S2 (supplementary material)] indicating slight to moderate weathering. Although CIA is an important index to understand the degree of weathering, chemical changes resulting from other processes such as diagenesis and metamorphism also need to be fully evaluated. Therefore, an alternative index Chemical Index of

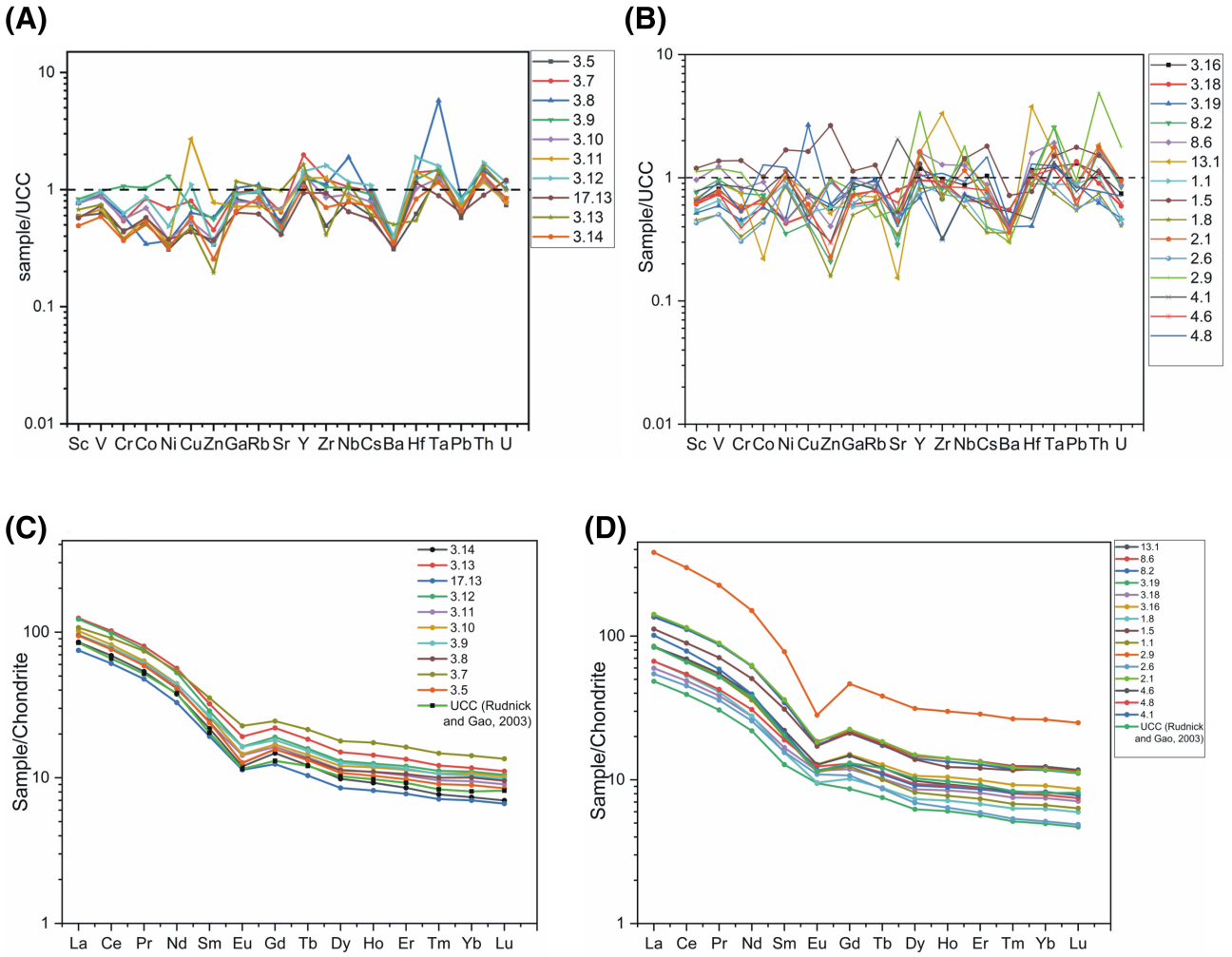

Fig. 6 Trace element concentrations of sandstones of (**A**) Dafla Formation (DF) and (**B**) Subansiri Formation (SF) normalized to the composition of the upper continental crust (after Rudnick and Gao 2003) and Chondrite-normalized REE Patterns (after Taylor and McLennan 1985) of the sandstones of (**C**) Dafla Formation and (**D**) Subansiri Formation in the study area. Sample numbers are given against each coloured graph in the legend

weathering (CIW, Harnois 1988) was used which eliminates K_2O from the equation also known as K_2O-free CIA or CIA-K. It does not account for the K associated with feldspars and is a measure of the extent of conversion of feldspars to clays. The average CIW values for the sandstones of DF and SF are 70.05 and 73.33 respectively, indicating that these sandstones were derived from moderately weathered source rocks. The Plagioclase Index of Alteration (PIA) (Fedo et al. 1995), is particularly suitable for monitoring of weathering in plagioclase feldspars and is also considered as a better tool in constraining weathering history of ancient sedimentary rocks than the CIA because K- metasomatism often reduces the CIA values. The PIA attains values of 50 in non-weathered rocks and close to 100 in clay minerals such as kaolinite, illite, and gibbsite (Nadlonek and Bojakowska 2018). The PIA values in DF and SF are 71.84 and 82.20 respectively [Tables S1 and S2 (supplementary material)] indicating moderate to intense weathering of plagioclase feldspars in both DF and SF.

The chemical weathering trend in rocks is evaluated by A–CN–K ternary plots (Nesbitt and Young 1982, 1984, 1989; Fedo et al. 1995; Nesbitt 2003), where $A = Al_2O_3$, $CN = CaO^* + Na_2O$, and $K = K_2O$ and all the values are in molecular proportions (Fig. 8A). Here, CaO* represents CaO in the silicate fractions. The versatility of this plot has been evaluated by many workers. A few of them are Fatima & Khan (2012), Tang et al. (2012); Armstrong-Altrin et al. (2013), Khan and Khan (2015), Khan et al. (2020). In this plot, the horizontal line representing CIA value equal to 50 (and which is parallel to the CN–K axis), represents the composition of natural feldspars and is known as the feldspar join. This line helps in constraining the initial composition of source rocks. During

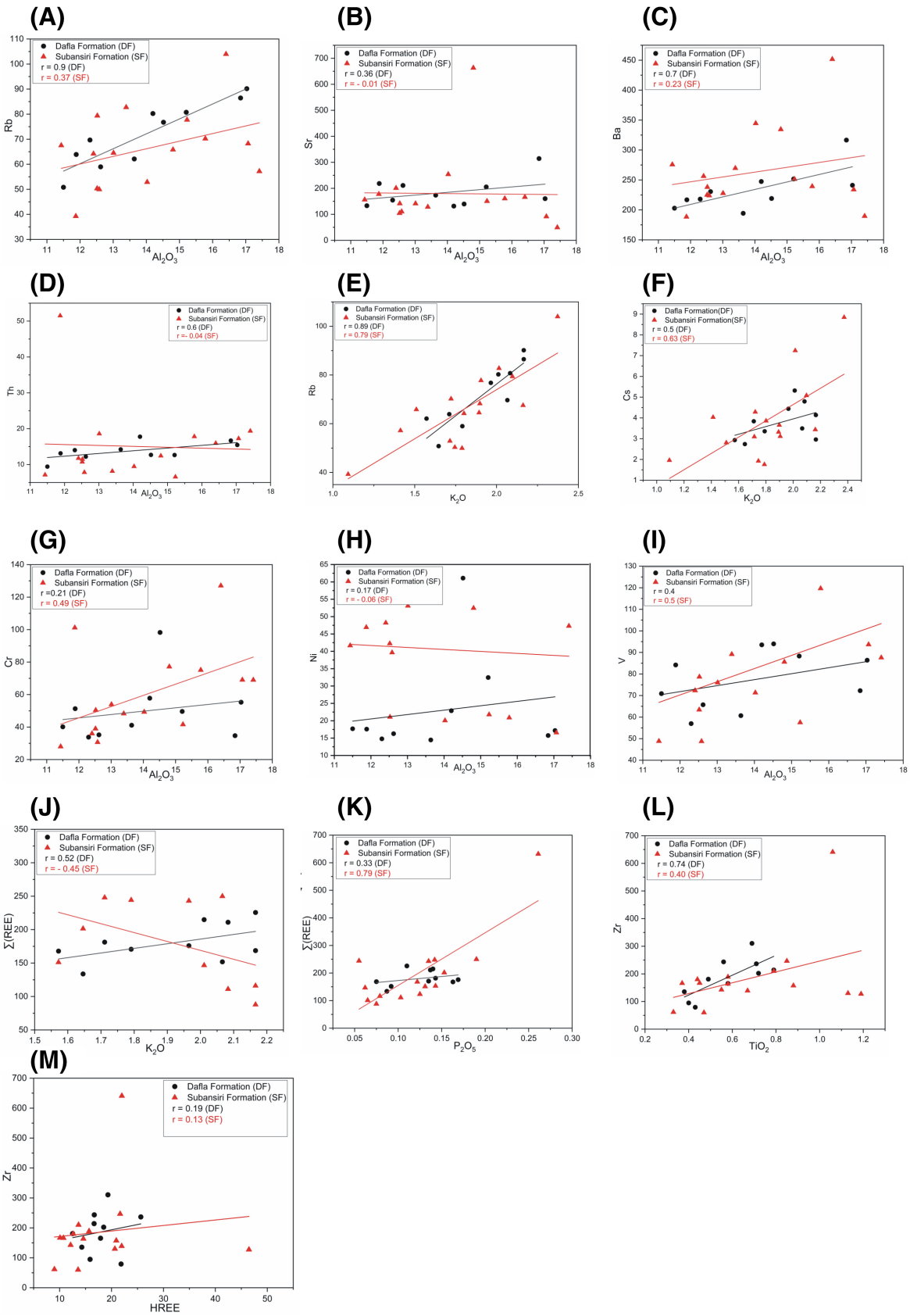
(A)
Dafla Formation (DF)
Subansiri Formation (SF)
r = 0.9 (DF)
r = 0.37 (SF)
Rb
Al2O3
(B)
Dafla Formation (DF)
Subansiri Formation (SF)
r = 0.36 (DF)
r = - 0.01 (SF)
Sr
Al2O3
(C)
Dafla Formation (DF)
Subansiri Formation (SF)
r = 0.7 (DF)
r = 0.23 (SF)
Ba
Al2O3
(D)
Dafla Formation (DF)
Subansiri Formation (SF)
r = 0.6 (DF)
r =- 0.04 (SF)
Th
Al2O3
(E)
Dafla Formation (DF)
Subansiri Formation (SF)
r = 0.89 (DF)
r = 0.79 (SF)
Rb
K2O
(F)
Dafla Formation(DF)
Subansiri Formation(SF)
r = 0.5 (DF)
r = 0.63 (SF)
Cs
K2O
(G)
Dafla Formation (DF)
Subansiri Formation (SF)
r =0.21 (DF)
r = 0.49 (SF)
Cr
Al2O3
(H)
Dafla Formation (DF)
Subansiri Formation (SF)
r = 0.17 (DF)
r = - 0.06 (SF)
Ni
Al2O3
(I)
Dafla Formation (DF)
Subansiri Formation (SF)
r = 0.4
r = 0.5 (SF)
V
Al2O3
(J)
Dafla Formation (DF)
Subansiri Formation (SF)
r = 0.52 (DF)
r = - 0.45 (SF)
∑(REE)
K2O
(K)
Dafla Formation (DF)
Subansiri Formation (SF)
r = 0.33 (DF)
r = 0.79 (SF)
∑(REE)
P2O5
(L)
Dafla Formation (DF)
Subansiri Formation (SF)
r = 0.74 (DF)
r = 0.40 (SF)
Zr
TiO2
(M)
Dafla Formation (DF)
Subansiri Formation (SF)
r = 0.19 (DF)
r = 0.13 (SF)
Zr
HREE

◀**Fig. 7** Bivariate plot of major oxides versus trace elements of DF and SF of the study area. Note that the datas used in this figures are LOI-free compositions

moderate chemical weathering, feldspars convert to muscovite, illite, and smectite, while intense chemical weathering leads to the formation of kaolinite and Al oxihydroxides. In general, the intensity of chemical weathering increases when there is a decrease in tectonic activity and/or warm and humid conditions prevail in the source region (Jacobson et al. 2003). The A–CN–K plot is also a valuable tool to estimate fresh rock compositions and for examining their weathering trends, since unweathered primary igneous rocks have CIA values close to 50 (Fedo et al. 1995). In the absence of K-metasomatism, the trendline of the sample data points would intersect the feldspar join at a point. This point indicates the proportion of plagioclase and K-feldspar of the fresh rock (or the parent rock). The quantity of K-enrichment and the palaeoweathering index before such enrichment can also be determined from the A–CN–K plot (Fedo et al. 1995). During K-metasomatism, sediments can take two different paths: (a) conversion of kaolinite to illite and/or (b) conversion of plagioclase to K-feldspar. Analyzed samples of the DF and SF of the present study do not show enrichment of K_2O. The average K_2O content of DF and SF are 1.92 and 1.81 respectively. The trends plot parallel to the A–CN line, this defining a non-steady-state trend of weathering. This non-steady-state weathering signifies a balanced rate of chemical weathering and erosion and produces sediments of similar composition over a long period (Nesbitt et al. 1997; Selvaraj and Chen 2006). The weathering trend suggests that the parent rock of the DF and SF had a more or less granodioritic chemical composition (Fig. 8A). The corrected CIA values (Fig. 8A) of DF ranges between 60 and 76.5, and in SF ranges between 68 and 90, suggesting mild to moderate weathering in DF and moderate to extreme weathering in SF.

Furthermore, molar proportions of Al_2O_3–K_2O, CaO*, and Na_2O were also plotted in the (A–K)–C–N diagram (Fedo et al. 1997) to understand and monitor the evolution of plagioclase weathering in the Neogene sediments. The left scale on the (A–K)–C–N triangle (Fig. 8B) corresponds to the plagioclase index of alteration ($PIA = [(Al_2O_3 - K_2O)/(Al_2O_3 + CaO^* + Na_2O - K_2O)] * 100$) of Fedo et al. (1997). The analyzed samples of DF indicate that sediments comprising the DF are weathered products of parent material enriched mostly in andesine (Ad). Similar analysis indicates that sediments comprising the SF are enriched mostly in andesine (Ad) and labradorite (La). The corrected PIA values of DF ranges between 60 and 82 suggesting moderate intensity of weathering of the feldspars while in SF the corrected PIA values range between 71 and 89 indicating moderate to intense weathering of the plagioclase feldspars. The effects of sediment recycling can also be understood by Rb/Sr and Th/U ratios. As Sr is a mobile element under certain conditions, weathering can thus increase the Rb/Sr ratio in sedimentary rocks. Intense weathering and sediment recycling are suggested by McLennan et al. (1993) in sediments having an Rb/Sr ratio of 0.5. The average Rb/Sr ratios of DF and SF samples were 0.45 and 0.49 respectively and thus are suggestive of sediment recycling up to a certain extent and further supports the derivation of these sediments from extremely weathered rocks such as phyllite and shale which are present in the hinterland towards the north of the study area (Selvaraj and Chen 2006). Besides, there is also an increase in the Th/U ratio as the intensity of weathering in source rocks increases (McLennan 2001). Values of Th/U above 3.8 are indicative of weathering history (McLennan et al. 1993). In the present study, the DF and SF show an average Th/U ratio of 5.7 and 6.95 respectively [Tables S1 and S2 (supplementary material)], which are higher than the UCC indicating moderate to an intense degree of chemical weathering in the source area and some amount of sediment recycling during the transport and sedimentary processes. The average concentration of Zr (DF: 186.3; SF: 185.41) which is high in these sandstones, suggests sediment derivation from zircon-rich source rocks. Zr/Sc and Th/Sc are important indexes of zircon enrichment and igneous chemical differentiation process respectively and preserve the signature of the provenance (Basu 1976). Typically, Th and Sc are incompatible and compatible elements to the igneous systems (McLennan et al. 1993). The plot of Th/Sc vs Zr/Sc (Fig. 9) suggests both addition of Zr and compositional variations in the sedimentary system. The ratio Zr/Sc is a measure of sediment recycling and sorting as Zr is concentrated in heavy minerals such as zircon (Basu 1976). Thus, the sandstones of the study area suggest sediment recycling along with compositional variations. This further indicates the addition of zircon from weathered sources like phyllite, slate, and mica-schists that are associated with the granitic material.

The trace element composition of sediments, in conjunction with their major element composition, can also be used to understand the paleoclimate conditions prevailing during sedimentation in a depositional basin (Bhatia and Crook 1986; Hatch and Leventhal 1992; Jones and Manning 1994; Rimmer 2004; Cao et al. 2012; Wang et al. 2017; Ding et al. 2018; Zuo et al. 2020). The Sr/Ba ratio has also been effectively used for interpreting paleosalinity conditions. Its values range between 0.6 and 1 for brackish water environments, and less than 0.6 in the case of the

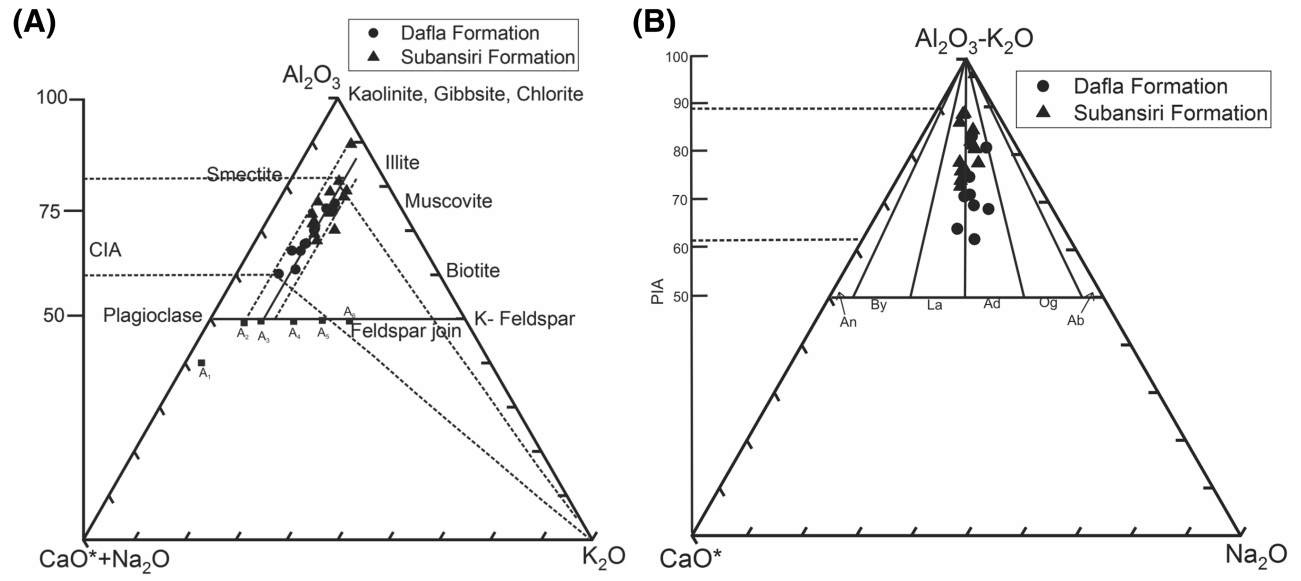

Fig. 8 **A** $Al_2O_3 - CaO^* + Na_2O - K_2O$ (A–CN–K) ternary diagram (after Nesbitt and Young 1984) of molecular ratios for the Neogene sandstones of the study area. Left scale indicates Chemical Index of Alteration (CIA). Solid line indicates the predicted weathering trend for granodiorite; dashed line shows the actual weathering of the samples. Average compositions of gabbro (A_1), tonalite (A_2), granodiorite (A_3), granite (A_4), A-type granite (A_5) and Charnockite (A_6) from Fedo et al. (1997); **B** ($Al_2O_3 - K_2O$) $- CaO^* - Na_2O$ [(A–K)–C–N] ternary diagram of the Neogene sandstones of the study area. Scale at the left indicates Plagioclase Index of Alteration (PIA) from Fedo et al. (1995). An: Anorthite; By: Bytownite; La: Labradorite; Ad: Andesine; Og: Oligoclase; Ab: Albite

freshwater environment in continental facies (Yuan et al. 2006). The Sr/Ba values in the DF range between 0.53 and 1 (average = 0.78) and in the SF it ranges between 0.26 and 1.98 (average = 0.66), suggesting the influence of both freshwater as well as brackish environments during deposition of the Neogene (DF and SF) sediments. Scheffler et al. (2006), Chen et al. (2018) and Zuo et al. (2020) have opined that the Rb/Sr ratio can also be effectively used to distinguish between humid and arid climatic conditions affecting sedimentation in a depositional basin. The Rb/Sr ratio increases under humid environmental conditions in a Continental Facies Basin (Zuo et al. 2020), and reduces under arid climatic conditions. In the case of the DF, the value of Rb/Sr varies between 0.28 and 0.61 while in SF the value ranges between 0.21 and 1.16. These values correlate with those from the near upper limit of Zuo et al. (2020) and with petrographic studies signifying humid climatic conditions. This probably signifies the prevalence of very extreme humid climatic conditions during the deposition of the Neogene (DF and SF) sediments. The versatility of the parameter V/(V + Ni) to understand the redox parameters of a depositional setup has been explained by many workers (Hatch and Leventhal 1992; Jones and Manning 1994; Zuo et al. 2020). The redox-sensitive elements V and Ni have anti-interference characters and are stable to judge paleo-redox conditions by the element ratio method (Zuo et al. 2020). A value of V/(V + Ni) < 0.5 indicates an oxidizing environment, while a value greater than 0.5 for the aforementioned parameter would point towards a reducing environment (Cai et al. 2009). In DF, the value of V/(V + Ni) ranges between 0.6 and 0.83, while in SF the value ranges between 0.53 and 0.85 [Tables S1 and S2 (supplementary material)]. This signifies the prevalence of reducing the environment during their deposition. Almost 80% of the analyzed samples in the DF have V/(V + Ni) value > 0.8. This indicates the prevalence of a very strong reducing environment during the deposition of the DF. Recent research has now shown

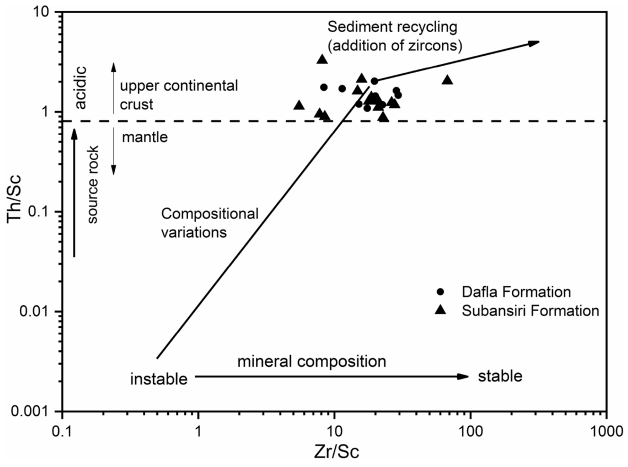

Fig. 9 Plot of Th/Sc versus Zr/Sc (after McLennan et al. 1993) of the studied sandstone samples showing concentration of zircon by sediment recycling as well as some variations in composition

Table 2 C-value for Paleoclimate Interpretation (Ding et al. 2018)

C-value	Paleoclimate interpretation (Ding et al. 2018)
0–0.2	Arid
0.2–0.4	Semi-arid
0.4–0.6	Semi-arid to semi-humid
0.6–0.8	Semi-humid
> 0.8	Humid

that Fe, Mn, V, Cr, Co, and Ni become enriched under moist and humid climatic conditions, while the increase in water alkalinity due to evaporation in arid climates facilitate saline minerals to precipitate, thereby leading to the concentration of elements such as Ca, Mg, Na, K, Ba, and Sr (Ding et al. 2018). Subsequently, the ratio $\sum$(Fe + Mn + Cr + Ni + V + Co)/$\sum$(Ca + Mg + Sr + Ba + K + Na) has been regarded as a climate proxy (termed as the "C-value") and has been widely used in the interpretation of paleoclimate data (Cao et al. 2012; Wang et al. 2017; Ding et al. 2018). The C-values for the Neogene sandstones range from 0.21 to 1.1 (Table 2). Amongst them, the DF samples have C-values ranging from 0.21 to 0.86 with an average of 0.69 indicating semi-humid climatic condition, while the SF samples have C-values ranging from 0.37 to 2.4 with an average of 1.02, indicating humid climatic conditions during the deposition of the sediments. The C-values also suggests the prevalence of highly humid climatic conditions at different moments during the deposition of the Neogene sediments. Short spells of arid and semi-arid climatic conditions are also indicated by few samples with C-values less than 0.2 and 0.4 respectively.

5.2 Provenance

The geochemical signatures of clastic sediments have long been used to understand their provenance characteristics (Taylor and McLennan 1985; Condie et al. 1992; Cullers 1995; Madhavaraju and Ramasamy 2002; Armstrong-Altrin et al. 2004, 2013). The source rock compositions of the clastic rocks can be inferred from Al_2O_3/TiO_2 since these major elements are considered immobile during weathering, transportation, and diagenesis (Spalletti et al. 2012; Absar and Sreenivas 2015; Zhou et al. 2015). The ratio increases from 3 to 8 for mafic rocks, 8 to 21 for intermediate rocks, and 21 to 70 for felsic igneous rocks (Hayashi et al. 1997). In the present study, the ratio varies from 20.22 to 34.35 (in DF) and 9.94 to 46.71 (in SF) which suggests that the probable source rocks were felsic igneous rocks for DF, and intermediate to felsic in compositions for SF. This result is also supported by the TiO_2 vs Ni binary plot (Floyd et al. 1989), which indicates that the sediments of DF were mainly derived from felsic source rocks and those comprising the SF were derived from rocks of felsic to intermediate compositions (Fig. 10A).

Certain trace elemental ratios e.g. Eu/Eu*, $(La/Lu)_{CN}$, La/Sc, La/Co, Th/Sc, Th/Co, and Cr/Th show marked differences in felsic and basic rocks, and hence they are used in determining the average composition of provenance (Wronkiewicz and Condie 1990; Cox et al. 1995; Cullers 1995). In the present study, these ratios are compared with those of sediments derived from felsic and basic

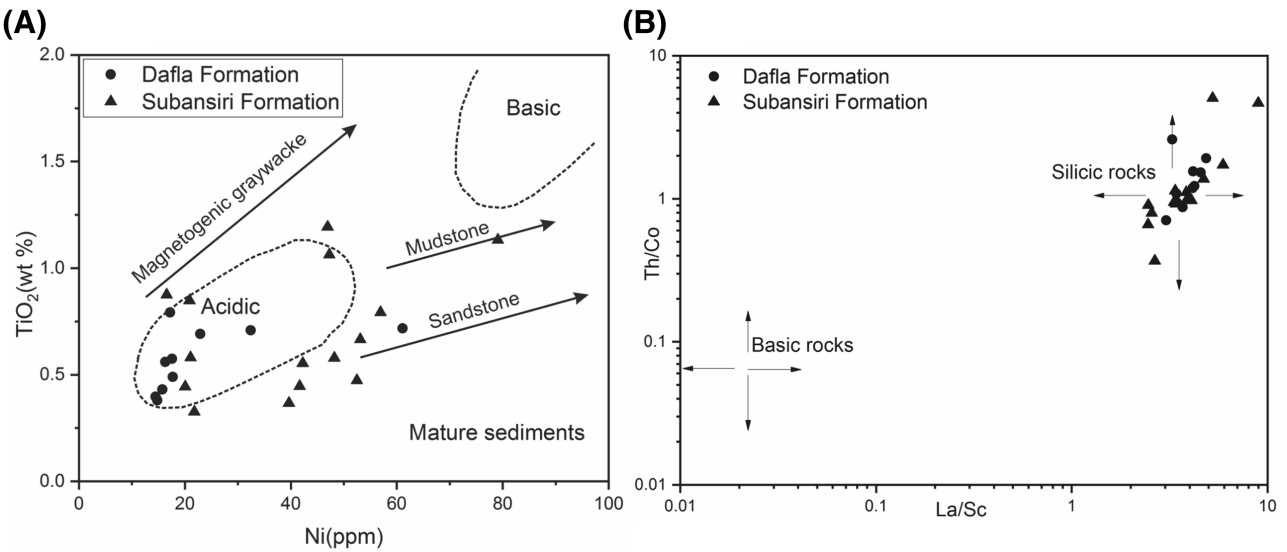

Fig. 10 Bivariate provenance plot of (**A**_ TiO_2 versus Ni (after Floyd et al. 1989) and (**b**) La/Sc versus Th/Co (after Cullers 2000)

rocks in fine fractions (Cullers 2000) as well as in UCC (Table 3). The comparison suggests that the values of these ratios are within the range of felsic rocks for both DF and SF. In addition, the La/Th and Th/Sc ratios are fairly constant in sedimentary rocks (2.4 and 0.9, respectively; Taylor and McLennan 1985). Furthermore, the plot of Th/Co versus La/Sc (Fig. 10B; Cullers 2000) also suggests that the sandstones were derived from felsic source rocks. The content of ferromagnesian trace elements like Cr, Ni, and V in sediments could indicate mafic rocks as their provenance (Cullers et al. 1979, 1997; Armstrong-Altrin et al. 2004). The high content of Cr and Ni (Cr > 150 ppm and Ni > 100 ppm) are indicative of ultramafic rocks in the source (Garver et al. 1996). The DF and SF of the present study area are significantly low in Cr and Ni content. The DF has an average of 49.72 and 23.0 ppm of Cr and Ni content respectively, while the SF has an average of 59.71 ppm and 40.52 ppm of Cr and Ni respectively, suggesting the absence of ultramafic rocks in the source area for both DF and SF.

Finally, the REE pattern and Eu anomaly in the sedimentary rocks provide important clues regarding the source rock characteristics (Taylor and McLennan 1985). Higher LREE/HREE ratios and negative Eu anomalies are generally found in felsic rocks, whereas mafic rocks exhibit lower LREE/HREE ratios and no or small Eu anomalies (Cullers 1994). The chondrite normalized REE patterns (Fig. 6C, D) show enrichment in LREE, almost flat HREE, and pronounced negative Eu anomaly, thereby suggesting that the source rocks are derived from the UCC and are felsic in composition.

The provenance of the study area is also analyzed through sandstone petrography since petrography of the sandstones allows the distinction of detrital and digenetic changes and also the study of grain textures, which helps in further supporting geochemical information (Rollinson 1993; Von Eynatten et al. 2003). The dominance of monocrystalline quartz grains over polycrystalline quartz grains indicates crystalline granite, granitic-gneiss, and sandstones as the sources (Pettijohn et al. 1972). The presence of feldspar also indicates the source rocks (Boggs 2009). The significantly low amounts of feldspar (low P/F ratio) together with the composition of quartz and lithic fragments suggest a recycled orogen provenance in the source area (Dickinson 1985). Generally, orthoclase and microcline feldspar are derived from granitic and/or gneissic sources whereas plagioclase feldspar is derived from low-grade metamorphic rocks (Deer et al. 1992; Pettijohn et al. 1972). The dominance of orthoclase feldspar with a low P/F ratio indicates the granitic and/or gneissic rocks as the source of these feldspars in the studied sandstones. The presence of both fresh, as well as weathered feldspars in the studied sandstones, indicates a humid climate and rugged topography in the provenance area (Folk 1968). The abundance of sedimentary and metamorphic lithic fragments in the studied sandstones and a meagre proportion of volcanic lithic fragments suggest that the source area was primarily metamorphic and sedimentary rocks. The presence of quartz-mica-schist, gneiss, quartzite, and phyllite points to medium to high grade and low-grade metamorphic source rocks respectively. Further, mudstone, siltstone, sandstone sedimentary lithic fragments point towards mixed argillites and arenites of sedimentary source terrain. Thus petrography and geochemistry of the studied sandstones suggest that the sediments were derived primarily from felsic to intermediate and low-grade metamorphic source rocks. The Bondila Gneiss, Dirang Formation, and Lumla Formation of the Lesser Himalayan terrain in the region and rocks belonging to the Higher Himalayas could form probable sources of sediment supply in the study area.

Table 3 Tabulated data of range of elemental ratios of sandstones of the study area and their comparison with ratios in similar fractions derived from felsic rocks, mafic rocks, and upper continental crust ([1]Cullers 1994, 2000; Cullers and Podkovyrov 2000; Cullers and Berendsen 1998; [2]McLennan 2001; Taylor and McLennan 1985)

Elemental ratio	Range in DF	Range in SF	Range in sediment from felsic sources[1]	Range in sediment from mafic sources[1]	Upper continental crust[2]
Eu/Eu*	0.65–0.77	0.61–0.90	0.40–0.94	0.71–0.95	0.63
$(La/Lu)_{CN}$	7.96–12.22	8.42–15.33	3.00–27.0	1.10–7.00	9.73
La/Sc	3.03–4.84	2.5–8.9	2.5–16.3	0.43–0.86	2.21
La/Co	1.96–5.88	1.1–13.01	1.8–13.8	0.14–0.38	1.76
Th/Sc	1.09–2.03	3.3–0.88	0.84–20.5	0.05–0.22	0.79
Th/Co	0.71–2.60	0.36–5.06	0.67–19.4	0.04–1.40	0.63
Cr/Th	2.1–7.74	1.96–7.96	4.00–15.0	25–500	7.76

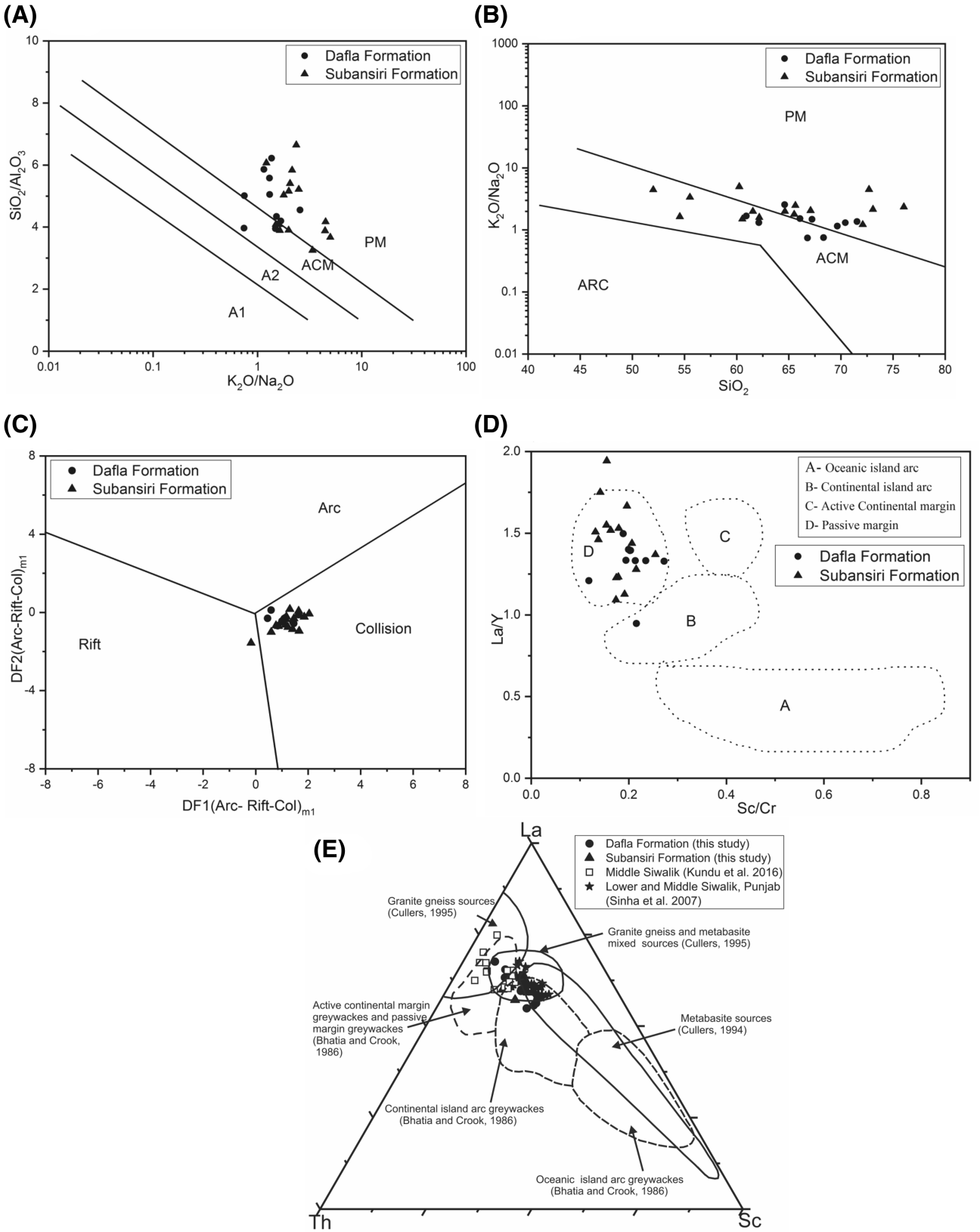
(A)
Dafla Formation
Subansiri Formation
PM
ACM
A2
A1
SiO2/Al2O3
K2O/Na2O
(B)
Dafla Formation
Subansiri Formation
PM
ACM
ARC
K2O/Na2O
SiO2
(C)
Dafla Formation
Subansiri Formation
Arc
Collision
Rift
DF2(Arc-Rift-Col)m1
DF1(Arc- Rift-Col)m1
(D)
A- Oceanic island arc
B- Continental island arc
C- Active Continental margin
D- Passive margin
Dafla Formation
Subansiri Formation
La/Y
Sc/Cr
(E)
Dafla Formation (this study)
Subansiri Formation (this study)
Middle Siwalik (Kundu et al. 2016)
Lower and Middle Siwalik, Punjab (Sinha et al. 2007)
Granite gneiss sources (Cullers, 1995)
Granite gneiss and metabasite mixed sources (Cullers, 1995)
Active continental margin greywackes and passive margin greywackes (Bhatia and Crook, 1986)
Metabasite sources (Cullers, 1994)
Continental island arc greywackes (Bhatia and Crook, 1986)
Oceanic island arc greywackes (Bhatia and Crook, 1986)
La
Th
Sc

◀**Fig. 11** Bivariate tectonic plot of **A** K_2O/Na_2O versus SiO_2/Al_2O_3 (after Maynard et al. 1982); **B** (K_2O/Na_2O) versus SiO_2 (after Roser and Korsch 1986); **C** Discriminant-function multi-dimensional diagram for high-silica clastic sediments (after Verma and Armstrong-Altrin 2013); **D** La/Y versus Sc/Cr (after Bhatia and Crook 1986) and **E** Ternary plot of La–Th–Sc for differentiation of tectonic setting and rock types (after Bhatia and Crook 1986; Cullers 1995). Note the samples of the present study, from Punjab (Sinha et al. 2007) and Lish valley, West Bengal (Kundu et al. 2016) show granite-gneiss and metabasic mixed provenance

5.3 Tectonic settings

The efficacy of using the geochemical composition of sediments to identify their source-rock composition and tectonic setting signatures, as well as the redistribution of various chemical constituents during and after their deposition, has since long been realized by many workers (Middleton 1960; Crook 1974; Schwab 1975; Maynard et al. 1982; Bhatia 1983; Roser and Korsch 1986; Cullers et al. 1988). Parameters such as $Fe_2O_3 + MgO$, TiO_2, Al_2O_3/SiO_2, K_2O/Na_2O, $Al_2O_3/(CaO + Na_2O)$, etc. were considered as discriminating factors for the identification of various tectonic settings of sediment deposition; other tectonic setting discrimination diagrams proposed by Bhatia (1983) and Roser and Korsch (1986) have been extensively used in sediment geochemistry to identify the tectonic setting of unknown sedimentary basins (Purevjav and Roser 2012; Yan et al. 2012). Lately, it has been realized that these discriminant diagrams are inconsistent with the geology of the associated study area (Valloni and Maynard 1981; Dostal and Keppie 2009). Furthermore, these discrimination diagrams were also evaluated based on geochemical data of Miocene to Holocene sediments, by other authors in recent times (Armstrong-Altrin and Verma 2005; Ryan and Williams 2007). They observe that the success rate for Bhatia (1983) and Roser and Korch (1986) diagrams were 0%–23% and 31.5%–52.3% respectively (Armstrong-Altrin and Verma 2005). Nevertheless, a few of the bivariate tectonic discriminant plots suggested by various workers have been considered in this study. The bivariate plot of K_2O/Na_2O vs SiO_2/Al_2O_3 (after Maynard et al. 1982) shows a greater concentration of points in the Passive Margin while a few samples plot near the boundary between Active Continental Margin setting and Passive Margin (Fig. 11A). Similarly, the log (K_2O/Na_2O) versus SiO_2 plot (after Roser and Korsch 1986) produces identical results, thereby suggesting mostly a Passive Margin with subordinate Active Continental Margin setup of deposition of the Neogene sediments (Fig. 11B). Recently, Verma and Armstrong-Altrin (2013) studied the geochemical compositions of Neogene-Quaternary sediments and based on the major-element composition, two discriminant functions have been proposed for the tectonic discrimination of siliciclastic sediments for high-silica [(SiO_2)adj = 63%–95%] and low-silica [(SiO_2) adj = 35%–63%] types. Three main tectonic settings are proposed, namely, the island or continental arc, the continental rift, and the collision tectonic setup. A bivariate plot of DF1 and DF2 for the Neogene sediments of the present study area indicates a collisional tectonic setting during the deposition of the sediments (Fig. 11C). The immobile trace elements La, Nd, Th, Zr, Nb, Y, Sc, and Co have also been utilized in the discrimination of tectonic settings of sediments. Significant amongst them are the bivariate plots and ternary plots of Bhatia and Crook 1986 and Cullers 1995. The plot of Sc/Cr versus La/Y (Fig. 11D; after Bhatia and Crook 1986) suggests a passive margin tectonic setting of deposition of the Neogene sediments. The tectonic environments of sedimentation can also be inferred based on the REE distribution in clastic sediments (Bhatia 1985; McLennan and Taylor 1991; McLennan et al. 1993). Bhatia (1985) documented that Passive Margin settings are typically characterized by uniform REE patterns similar to average UCC (Rudnick and Gao 2003) with pronounced negative Eu anomaly, while sediments from Active Continental Margin display fractionated REE patterns with a wide range of negative Eu anomaly. In the present study, the DF and SF samples show enrichment of LREE with pronounced negative Eu anomalies ($Eu/Eu^* = 0.6–0.9$ for DF and 0.5–0.9 for SF) and relatively flat HREE patterns (Fig. 6C, D), which is suggestive of a Passive Margin tectonic setting for the Neogene (Dafla and Subansiri formation) sediments. Thus a Passive Margin with subordinate active margin setup is inferred from the various plots of major and trace elements which also points to the rocks of a pre-collision continental margin (Kundu et al. 2016).

The sandstones of the present area are also compared with the study of Siwalik sediments carried out in Western Himalaya by Sinha et al. (2007) and in Eastern Himalaya by Kundu et al. (2016), differentiate the different tectonic settings and rock types. The ternary plot of La-Th-Sc (Fig. 11E; after Bhatia and Crook 1986; Cullers 1995) in the present study show granite-gneiss and metabasic mixed source rocks which is in similarity with conclusions on the provenance of sediments in Western Himalaya (Sinha et al. 2007) and Eastern Himalaya (Kundu et al. 2016).

6 Conclusions

The geochemical analysis of the Neogene sandstones of Dafla and Subansiri Formation was undertaken to study the lithology, paleoweathering, provenance, and tectonic settings. The main conclusions are summarized as:

1. Sandstones of the Dafla and Subansiri Formation were classified as greywacke and litharenite based on the

dominance of quartz and lithic fragments over the minor presence of feldspar.
2. The weathering indices like CIA, CIW indicate that the source rock was affected by moderate to intense chemical weathering probably in a humid climatic condition.
3. The ratios of various trace elements including REE, chondrite-normalized REE patterns, and petrographic results collectively suggest that the sandstones of Dafla and Subansiri Formation were derived dominantly from felsic igneous rocks in an upper continental crustal setting.
4. The geochemical signatures as well as thin-section petrography of the sandstones belonging to the Dafla and Subansiri Formation occurring in the East and West Siang Districts of Arunachal Pradesh, India indicates a mixed provenance comprising of granite-gneiss and/or recycled sedimentary and metasedimentary rocks. The Bomdila Gneiss and Lumla / Dirang Formations of the Lesser Himalayas, as well as formations belonging to the Higher Himalayan sequences lying to the north of the study area, must have been significant contributors to Neogene sedimentation in the region.

Supplementary Information The online version contains supplementary material available at https://doi.org/10.1007/s11631-021-00497-9.

Acknowledgements The authors wish to thank the Head of the Department of Geological Sciences, Gauhati University for providing the necessary facilities to undertake the work. The Director and Head of the Geochemical Division, CSIR- National Geophysical Research Institute, Hyderabad is also thankfully acknowledged for granting necessary permission to undertake geochemical analysis of the samples. Constructive suggestions from all anonymous reviewers of the manuscript is also thankfully acknowledged.

Funding Self-funded.

Availability of data and material All data generated and analyzed during this study are included in this published article and its supplementary information files.

Code availability No computer programmes were utilized.

Declarations

Conflict of interest The authors declare that they have no conflict of interest.

Ethics approval The data and interpretations cited in this paper are a part of our geological research in the region.

Consent to participate Both the authors have mutually agreed to write the paper and define their individual contribution to the paper.

Consent for publication Yes.

References

Absar N, Sreenivas B (2015) Petrology and geochemistry of greywackes of the ~1.6 Ga Middle Aravalli Supergroup, northwest India: evidence for active margin processes. International Geology Review 57(2):134–158

Ali S, Stattegger K, Garbe-Schönberg D, Frank M, Kraft S, Kuhnt W (2014) The provenance of Cretaceous to Quaternary sediments in the Tarfaya basin, SW Morocco: evidence from trace element geochemistry and radiogenic Nd–Sr isotopes. J Afr Earth Sc 90:64–76

Armstrong-Altrin JS, Verma SP (2005) Critical evaluation of six tectonic setting discrimination diagrams using geochemical data of Neogene sediments from known tectonic settings. Sed Geol 177(1–2):115–129

Armstrong-Altrin JS, Lee YI, Verma SP, Ramasamy S (2004) Geochemistry of sandstones from the Upper Miocene Kudankulam Formation, southern India: implications for provenance, weathering, and tectonic setting. J Sediment Res 74(2):285–297

Armstrong-Altrin JS, Nagarajan R, Madhavaraju J, Rosalez-Hoz L, Lee YI, Balaram V, Cruz-Martínez A, Avila-Ramirez G (2013) Geochemistry of the Jurassic and upper Cretaceous shales from the Molango Region, Hidalgo, Eastern Mexico: implications for source-area weathering, provenance, and tectonic setting. CR Geosci 345:185–202

Armstrong-Altrin JS, Nagarajan R, Balaram V, Natalhy-Pineda O (2015) Petrography and geochemistry of sands from the Chachalacas and Veracruz beach areas, western Gulf of Mexico, Mexico: constraints on provenance and tectonic setting. J S Am Earth Sci 64:199–216

Auden JB (1934) Geology of the Krol Belt. Records of Geological Survey of India, Simla, p 67

Basu A (1976) Petrology of Holocene fluvial sand derived from plutonic source rocks; implications to paleoclimatic interpretation. J Sediment Petrol 46:694–709

Bhatia MR (1983) Plate tectonics and geochemical composition of sandstones. J Geol 91(6):611–627

Bhatia MR (1985) Rare earth element geochemistry of Australian Paleozoic graywackes and mudrocks: provenance and tectonic control. Sed Geol 45(1–2):97–113

Bhatia MR, Crook KA (1986) Trace element characteristics of graywackes and tectonic setting discrimination of sedimentary basins. Contrib Miner Petrol 92(2):181–193

Bhattacharjee S, Nandy S (2009) Geology of the western Arunachal Himalaya in parts of Tawang and west Kameng districts, Arunachal Pradesh. J Geol Soc India 73:589–590

Boggs S (2009) Petrology of sedimentary rocks, 2nd edn. Cambridge University Press, Cambridge. https://doi.org/10.1017/CBO9780511626487

Cai GQ, Guo F, Liu XT (2009) Carbon and oxygen isotope characteristics and palaeoenvironmental implications of lacustrine carbonate rocks from the Shahejie formation in the Dongying Sag. Earth Environ 37:347–354

Cao J, Wu M, Chen Y, Hu K, Bian L, Wang L, Zhang Y (2012) Trace and rare earth element geochemistry of Jurassic mudstones in the northern Qaidam Basin, northwest China. Geochemistry 72(3):245–252

Chen J, Huang WH, He MQ (2018) Elemental geochemistry characteristics of mudstones from Benxi formation to lower Shihezi formation in southeastern Ordos Basin. Geoscience 32:240–250

Chirouze F, Dupont-Nivet G, Huyghe P, van der Beek P, Chakraborti T, Bernet M, Erens V (2012) Magnetostratigraphy of the Neogene Siwalik Group in the far eastern Himalaya: Kameng section, Arunachal Pradesh, India. J Asian Earth Sci 44:117–135

Chirouze F, Huyghe P, Van Der Beek P, Chauvel C, Chakraborty T, Dupont-Nivet G, Bernet M (2013) Tectonics, exhumation, and drainage evolution of the eastern Himalaya since 13 Ma from detrital geochemistry and thermochronology, Kameng River Section. Arunachal Pradesh Bull 125(3–4):523–538

Condie KC, Noll PD Jr, Conway CM (1992) Geochemical and detrital mode evidence for two sources of Early Proterozoic sedimentary rocks from the Tonto Basin Supergroup, central Arizona. Sed Geol 77(1–2):51–76

Cox R, Lowe DR, Cullers RL (1995) The influence of sediment recycling and basement composition on evolution of mudrock chemistry in the southwestern United States. Geochim Cosmochim Acta 59(14):2919–2940

Crook KAW (1974) Lithogenesis and geotectonics: the significance of compositional variations in flysch arenites graywackes. In: Dott RH, Shaver RH (eds) Modern and Ancient geosynclinal sedimentation, vol 19. SEPM Special Publication, Broken Arrow, pp 304–310

Cullers RL (1994) The controls on the major and trace element variation of shales, siltstones, and sandstones of Pennsylvanian-Permian age from uplifted continental blocks in Colorado to platform sediment in Kansas, USA. Geochim Cosmochim Acta 58(22):4955–4972

Cullers RL (1995) The controls on the major-and trace-element evolution of shales, siltstones and sandstones of Ordovician to Tertiary age in the Wet Mountains region, Colorado, USA. Chem Geol 123(1–4):107–131

Cullers RL (2000) The geochemistry of shales, siltstones and sandstones of Pennsylvanian-Permian age, Colorado, USA: implications for provenance and metamorphic studies. Lithos 51(3):181–203

Cullers R, Chaudhuri S, Kilbane N, Koch R (1979) Rare-earths in size fractions and sedimentary rocks of Pennsylvanian-Permian age from the mid-continent of the USA. Geochim Cosmochim Acta 43(8):1285–1301

Cullers RL, Basu A, Suttner LJ (1988) Geochemical signature of provenance in sand-size material in soils and stream sediments near the Tobacco Root batholith, Montana, USA. Chem Geol 70(4):335–348

Cullers RL, Berendsen P (1998) The provenance and chemical variation of sandstones associated with the Mid-continent Rift System, USA. Eur J Mineral 10(5):987–1002

Cullers RL, Bock B, Guidotti C (1997) Elemental distributions and neodymium isotopic compositions of Silurian metasediments, western Maine, USA: redistribution of the rare earth elements. Geochim Cosmochim Acta 61(9):1847–1861

Cullers RL, Podkovyrov VN (2000) Geochemistry of the Mesoproterozoic Lakhanda shales in southeastern Yakutia, Russia: implications for mineralogical and provenance control, and recycling. Precambr Res 104(1–2):77–93

Deer WA, Howie RA, Zussman J (1992) An introduction to the rock-forming minerals, vol 696. Longman, Essex

Dickinson WR (1985) Interpreting provenance relations from detrital modes of sandstones. In Provenance of arenites: NATO ASI Series. Springer, Dordrecht, pp 333–362

Ding J, Zhang J, Tang X, Huo Z, Han S, Lang Y, Zheng Y, Li X, Liu T (2018) Elemental geochemical evidence for depositional conditions and organic matter enrichment of black rock series strata in an inter-platform basin: The Lower Carboniferous Datang Formation, Southern Guizhou. Southwest China Minerals 8(11):509

Dostal J, Keppie JD (2009) Geochemistry of low-grade clastic rocks in the Acatlán Complex of southern Mexico: Evidence for local provenance in felsic–intermediate igneous rocks. Sed Geol 222(3–4):241–253

Etemad-Saeed N, Hosseini-Barzi M, Adabi MH, Sadeghi A, Houshmandzadeh A (2015) Provenance of Neoproterozoic sedimentary basement of northern Iran, Kahar Formation. J Afr Earth Sc 111:54–75

Fatima S, Khan MS (2012) Petrographic and geochemical characteristics of Mesoproterozoic Kumbalgarh clastic rocks, NW Indian shield: implications for provenance, tectonic setting, and crustal evolution. Int Geol Rev 54(10):1113–1144

Fedo CM, Wayne Nesbitt H, Young GM (1995) Unraveling the effects of potassium metasomatism in sedimentary rocks and paleosols, with implications for paleoweathering conditions and provenance. Geology 23(10):921–924

Fedo CM, Young GM, Nesbitt HW, Hanchar JM (1997) Potassic and sodic metasomatism in the southern province of the Canadian Shield: evidence from the Paleoproterozoic Serpent Formation, Huronian Supergroup. Can Precambrian Res 84(1–2):17–36

Feng R, Kerrich R (1990) Geochemistry of fine-grained clastic sediments in the Archean Abitibi greenstone belt, Canada: implications for provenance and tectonic setting. Geochim Cosmochim Acta 54(4):1061–1081

Floyd PA, Winchester JA, Park RG (1989) Geochemistry and tectonic setting of Lewisian clastic metasediments from the Early Proterozoic Loch Maree Group of Gairloch, NW Scotland. Precambrian Res 45(1–3):203–214

Folk RL (1968) Petrology of sedimentary rocks. Hemphill publishing company, Austin, Texas

Gansser A (1964) The geology of the Himalayas. Wiley International Science, New York, p 289

Garver JI, Royce PR, Smick TA (1996) Chromium and nickel in shale of the Taconic foreland: a case study for the provenance of fine-grained sediments with an ultramafic source. J Sediment Res 66:100–106

Geological Survey of India (1989) Key papers presented in group discussion on tertiary stratigraphy of North Eastern India: held at Shillong, April 1985 (No. 23). Geol Surv India Spec Publ 23:1–43

Harnois L (1988) The CIW index: A new chemical index of weathering. Sed Geol 55(3):319–322

Hatch JR, Leventhal JS (1992) Relationship between inferred redox potential of the depositional environment and geochemistry of the Upper Pennsylvanian (Missourian) Stark Shale Member of the Dennis Limestone, Wabaunsee County, Kansas, USA. Chem Geol 99(1–3):65–82

Hayashi KI, Fujisawa H, Holland HD, Ohmoto H (1997) Geochemistry of ~1.9 Ga sedimentary rocks from northeastern Labrador, Canada. Geochim Cosmochim Acta 61(19):4115–4137

Herron MM (1988) Geochemical classification of terrigenous sands and shales from core or log data. J Sediment Petrol 58:820–829

Jacobson AD, Blum JD, Chamberlain CP, Craw D, Koons PO (2003) Climatic and tectonic controls on chemical weathering in the New Zealand Southern Alps. Geochim Cosmochim Acta 67(1):29–46

Jones B, Manning DA (1994) Comparison of geochemical indices used for the interpretation of palaeoredox conditions in ancient mudstones. Chem Geol 111(1–4):111–129

Karunakaran C, Ranga Rao A (1976) Status of exploration for hydrocarbons in the Himalayan region- Contributions to stratigraphy and structure. In: International Himalayan Geological Seminar India, Section III, ONGC, pp 1–72

Kesari GK (2010) Geology and Mineral Resources of Arunachal Pradesh. Geological Survey of India Miscellaneous Publication, vols. 30 Part IV, I (i). Geological Survey of India, Guwahati, Arunachal Pradesh 54

Khan T, Khan MS (2015) Clastic rock geochemistry of Punagarh basin, trans-Aravalli region, NW Indian shield: implications for

paleoweathering, provenance, and tectonic setting. Arab J Geosci 8(6):3621–3644
Khan T, Sarma DS, Somasekhar V, Ramanaiah S, Reddy NR (2020) Geochemistry of the Palaeoproterozoic quartzites of Lower Cuddapah Supergroup, South India: implications for the palaeoweathering, provenance, and crustal evolution. Geol J 55(2):1587–1611
Krishna AK, Murthy NN, Govil PK (2007) Multielement analysis of soils by wavelength-dispersive X-ray fluorescence spectrometry. At Spectrosc 28(6):202–214
Kumar G (1997) Geology of Arunachal Pradesh. Geological Society of India, Bangalore, p 217
Kundu A, Matin A, Eriksson PG (2016) Petrography and geochemistry of the Middle Siwalik sandstones (tertiary) in understanding the provenance of sub-Himalayan sediments in the Lish River Valley, West Bengal, India. Arab J Geosci 9(2):162
Lang KA, Huntington KW, Burmester R, Housen B (2016) Rapid exhumation of the eastern Himalayan syntaxis since the late Miocene. Bulletin 128(9–10):1403–422
Madhavaraju J (2015) Geochemistry of late cretaceous sedimentary rocks of the Cauvery Basin, South India: constraints on paleoweathering, provenance, and end cretaceous environments. In: Ramkumar M (ed) Chemostratigraphy: concepts, Techniques and Applications, 1st edn. Elsevier, Amsterdam, pp 185–214
Madhavaraju J, Ramasamy S (2002) Petrography and geochemistry of Late Maastrichtian-Early Palaeocene sediments of Tiruchirapalli, Tamil Nadu-Palaeoweathering and provenance implications. J Geol Soc India 59:133–142
Masuda A (1962) Regularities in variation of relative abundances of lanthanide elements and an attempt to analyze separation index patterns of some minerals. J Earth Sci Nagoya Univ 10:173–187
Mathur LP, Evans P (1964) Oil in India. In: International geological congress, 22nd session. New Delhi, India, pp 1–84
Maynard JB, Valloni R, Yu HS (1982) Composition of modern deep-sea sands from arc-related basins. Geol Soc Lond Spec Publ 10(1):551–561
McLennan SM (1989) Rare earth elements in sedimentary rocks; influence of provenance and sedimentary processes. Rev Mineral Geochem 21:169–200
McLennan SM, Taylor SR (1991) Sedimentary rocks and crustal evolution: tectonic setting and secular trends. J Geol 99(1):1–21
McLennan SM, Taylor SR, Eriksson KA (1983) Geochemistry of Archean shales from the Pilbara Supergroup, western Australia. Geochim Cosmochim Acta 47(7):1211–1222
McLennan SM, Hemming S, McDaniel DK, Hanson GN (1993) Geochemical approaches to sedimentation, provenance, and tectonics. In: Johnsson MJ, Basu A (eds) Processes controlling the composition of clastic sediments. Special papers - Geological Society of America, pp. 21–40
McLennan SM (2001) Relationships between the trace element composition of sedimentary rocks and upper continental crust. Geochem Geophys Geosyst 2(4)
Middleton GV (1960) Chemical composition of sandstones. Geol Soc Am Bull 71(7):1011–1026
Nadlonek W, Bojakowska I (2018) Variability of chemical weathering indices in modern sediments of the Vistula and Odra Rivers, (Poland). Appl Ecol Environ Res 16:2453–2473
Nesbitt H, Young GM (1982) Early Proterozoic climates and plate motions inferred from major element chemistry of lutites. Nature 299(5885):715–717
Nesbitt HW, Young GM (1984) Prediction of some weathering trends of plutonic and volcanic rocks based on thermodynamic and kinetic considerations. Geochim Cosmochim Acta 48(7):1523–1534
Nesbitt HW, Young GM (1989) Formation and diagenesis of weathering profiles. J Geol 97(2):129–147
Nesbitt HW, Fedo CM, Young GM (1997) Quartz and feldspar stability, steady and non-steady-state weathering, and petrogenesis of siliciclastic sands and muds. J Geol 105(2):173–192
Nesbitt HW (2003) Petrogenesis of siliciclastic sediments and sedimentary rocks. In: Lentz DR (ed) Geochemistry of sediments and sedimentary rocks. Evolutionary considerations to mineral deposit-forming environments, vol 4. Geological Association of Canada, Geotex, pp 439–451
Odoma AN, Obaje NG, Omada JI, Idakwo SO, Erbacher J (2015) Mineralogical, chemical composition and distribution of rare earth elements in clay-rich sediments from southeastern Nigeria. J Afr Earth Sc 102:50–60
Pettijohn FJ, Potter PE, Siever R (1972) Petrography of common sands and sandstones. In: Sand and sandstone. Springer, New York, pp 175–260
Purevjav N, Roser B (2012) Geochemistry of Devonian-Carboniferous clastic sediments of the T setserleg terrane, Hangay B asin, Central Mongolia: provenance, source weathering, and tectonic setting. Island Arc 21(4):270–287
Rahman MJJ, Sayem ASM, McCann T (2014) Geochemistry and provenance of the Miocene sandstones of the Surma group from the Sitapahar anticline, Southeastern Bengal Basin, Bangladesh. J Geol Soc India 83(4):447–456
Ramachandran A, Madhavaraju J, Ramasamy S, Lee YI, Rao S, Chawngthu DL, Velmurugan K (2016) Geochemistry of Proterozoic clastic rocks of the Kerur Formation of Kaladgi Badami Basin, North Karnataka, South India: implications for paleoweathering and provenance. Turkish J Earth Sci 25:126–144
Ramakrishnan M, Vaidyanandhan R (2008) Geology of India, vol 1. Geological Society of India, Bangalore, pp 335–365
Rimmer SM (2004) Geochemical paleoredox indicators in Devonian-Mississippian black shales, central Appalachian Basin (USA). Chem Geol 206(3–4):373–391
Rollinson HR (1993) Using geochemical data: evaluation, presentation, interpretation. Longman Group UK Ltd, London, p 275
Roser BP, Korsch RJ (1986) Determination of tectonic setting of sandstone-mudstone suites using SiO_2 content and K_2O/Na_2O ratio. J Geol 94(5):635–650
Rudnick RL, Gao S (2003) Composition of the continental crust, the crust. In: Heinrich DH, Turekian KK (eds) Treatise on geochemistry. Pergamon, Oxford, pp 1–64
Ryan KM, Williams DM (2007) Testing the reliability of discrimination diagrams for determining the tectonic depositional environment of ancient sedimentary basins. Chem Geol 242(1–2):103–125
Saini NK, Mukherjee PK, Rathi MS, Khanna PP (2000) Evaluation of energy-dispersive x-ray fluorescence spectrometry in the rapid analysis of silicate rocks using pressed powder pellets. X-Ray Spectrom 29(2):166–172
Satyanarayanan M, Balaram V, Sawant SS, Subramanyam KSV, Krishna GV (2014) High precision multielement analysis on geological samples by HR-ICP-MS. In SK Aggarwal, PG Jaison, A Sarkar (Eds) 28th ISMAS symposium cum workshop on mass spectrometry. Indian Society for Mass Spectrometry, Mumbai, pp 181–184
Scheffler K, Buehmann D, Schwark L (2006) Analysis of late Palaeozoic glacial to postglacial sedimentary successions in South Africa by geochemical proxies–Response to climate evolution and sedimentary environment. Palaeogeogr Palaeoclimatol Palaeoecol 240(1–2):184–203
Schwab FL (1975) Framework mineralogy and chemical composition of continental margin-type sandstone. Geology 3(9):487–490
Sekhose K, Prajapati S, Jain A (2016) Final report on specialized thematic mapping to study the evolution of Gondwana Supergroup and Siwalik group in parts of Papum Pare and Lower

Subansiri districts, Arunachal Pradesh, Geological Survey of India. In: Report., Mission I-A/North Eastern Region 155

Selvaraj K, Chen CT (2006) Moderate chemical weathering of subtropical Taiwan: constraints from solid-phase geochemistry of sediments and sedimentary rocks. J Geol 114(1):101–116

Singh G (1977) On the discovery of vertebrate fossil from the Upper Tertiary of Subansiri district, Arunachal Pradesh. Indian Minerals 29:65–67

Sinha S, Islam R, Ghosh SK, Kumar R, Sangode SJ (2007) Geochemistry of Neogene Siwalik mudstones along Punjab reentrant, India: implications for source-area weathering, provenance and tectonic setting. Curr Sci 92(8):1103–1113

Sinha S, Ghosh SK, Kumar R, Islam R, Sanyal P, Sangode SJ (2008) Role of tectono-climatic factors in the Neogene Himalayan Foreland sediments: petrology and geochemical approach, Kangra Sub-basin. J Geol Soc India 71:787–807

Spalletti LA, Limarino CO, Piñol FC (2012) Petrology and geochemistry of Carboniferous siliciclastics from the Argentine Frontal Cordillera: a test of methods for interpreting provenance and tectonic setting. J S Am Earth Sci 36:32–54

Tang DM, Qin KZ, Sun H, Su BX, Xiao QH (2012) The role of crustal contamination in the formation of Ni–Cu sulfide deposits in Eastern Tianshan, Xinjiang, Northwest China: evidence from trace element geochemistry, Re–Os, Sr–Nd, zircon Hf–O, and sulfur isotopes. J Asian Earth Sci 49:145–160

Taral S, Kar N, Chakraborty T (2017) Wave-generated structures in the Siwalik rocks of Tista valley, eastern Himalaya: implication for regional palaeogeography. Curr Sci 113(5):889–901

Taylor SR, McLennan SM (1985) The continental crust: its composition and evolution. Blackwell, Oxford, p 312

Tripathi C, Gaur RK, Singh S (1988) A note on the occurrence of Nummulitic limestone in East Siang district, Arunachal Pradesh. Geol Surv India Spec Publ 11(1):252–254

Valdiya KS (1980) Geology of Kumaon Lesser Himalaya. Wadia Institute of Himalayan Geology, Dehra Dun, p 292

Valdiya KS (2010) The making of India: geodynamic evolution. MacMillan, New Delhi, p 816

Valloni R, Maynard JB (1981) Detrital modes of recent deep-sea sands and their relation to tectonic setting: a first approximation. Sedimentology 28(1):75–83

Verma SP, Armstrong-Altrin JS (2013) New multi-dimensional diagrams for tectonic discrimination of siliciclastic sediments and their application to Precambrian basins. Chem Geol 355:117–133

Von Eynatten H, Barcelo-Vidal C, Pawlowsky-Glahn V (2003) Composition and discrimination of sandstones: a statistical evaluation of different analytical methods. J Sediment Res 73(1):47–57

Wadia DN (1953) Geology of India. Macmilan and Company Ltd, London

Wang Z, Fu X, Feng X, Song C, Wang D, Chen W, Zeng S (2017) Geochemical features of the black shales from the Wuyu Basin, southern Tibet: implications for palaeoenvironment and palaeoclimate. Geol J 52(2):282–297

Wronkiewicz DJ, Condie KC (1990) Geochemistry and mineralogy of sediments from the Ventersdorp and Transvaal Supergroups, South Africa: cratonic evolution during the early Proterozoic. Geochim Cosmochim Acta 54(2):343–354

Yan Z, Wang Z, Yan Q, Wang T, Guo X (2012) Geochemical constraints on the provenance and depositional setting of the Devonian Liuling Group, East Qinling Mountains, Central China: implications for the tectonic evolution of the Qinling Orogenic Belt. J Sediment Res 82(1):9–20

Yin A, Dubey CS, Kelty TK, Gehrels GE, Chou CY, Grove M, Lovera O (2006) Structural evolution of the Arunachal Himalaya and implications for asymmetric development of the Himalayan orogen. Curr Sci Bangalore 90:195–206

Yuan WF, Chen SY, Zeng CM (2006) Study on marine transgression of paleogene Shahejie Formation in Jiyang depression. Acta Petrolei Sinica 27(4):40–44 (**in Chinese, with English abstract**)

Zaid SM (2015a) Geochemistry of sandstones from the Pliocene Gabir Formation, north Marsa Alam, Red Sea, Egypt: implication for provenance, weathering and tectonic setting. J Afr Earth Sc 102:1–17

Zaid SM (2015b) Geochemistry of sands along the Ain Soukhna and Ras Gharib beaches, Gulf of Suez, Egypt: implications for provenance and tectonic setting. Arab J Geosci 8(12):10481–10496

Zhou JB, Wang B, Wilde SA, Zhao GC, Cao JL, Zheng CQ, Zeng WS (2015) Geochemistry and U-Pb zircon dating of the Toudaoqiao blueschists in the Great Xing'an Range, northeast China, and tectonic implications. J Asian Earth Sci 97:197–210

Zuo X, Li C, Zhang J, Ma G, Chen P (2020) Geochemical characteristics and depositional environment of the Shahejie Formation in the Binnan Oilfield. China J Geophys Eng 17(3):539–551